iScience

CellPress
OPEN ACCESS

Review

High-entropy materials for energy-related applications

Maosen Fu,[1,*] Xiao Ma,[1,*] Kangning Zhao,[2] Xiao Li,[2] and Dong Su[2,*]

SUMMARY

High-entropy materials (HEMs), including high-entropy alloys (HEAs), high-entropy oxides (HEOs), and other high-entropy compounds, have gained significant interests over the past years. These materials have unique structures with the coexistence of antisite disordering and crystal periodicity, which were originally investigated as structural materials. Recently, they have emerged for energy-related applications, such as catalysis, energy storage, etc. In this work, we review the research progress of energy-related applications of HEMs. After an introduction on the background, theory, and syntheses of HEMs, we survey their applications including electrocatalysis, batteries, and others, aiming to retrieve the correlations between their structures and performances. In the end, we discussed the challenges and future directions for developing HEMs.

INTRODUCTION

High-entropy alloys (HEAs), also known as multi-principal element alloys, emerged into the academic literature in 2004 and have grown in applications and understanding since. They are multicomponent solid solution materials that contain five or more elements in near-equiatomic proportions to stabilize their structures by maximizing the configurational entropy (Cantor et al., 2004; Yeh et al., 2004). These unconventional structures provide opportunities for achieving unprecedented combinations of phase stability and mechanical performance (Ding et al., 2019; Gludovatz et al., 2014; Lei et al., 2018), especially overcoming the strength-ductility trade-off (Li et al., 2016). Although there are still arguments on if these multicomponent alloys are really stabilized by entropy or not (Löffler et al., 2019), we here call it HEAs for its popularity in the literature (George et al., 2019). It is believed that the excellent performances of HEAs are promoted by four "core effects": the high-entropy effect, the lattice distortion effect, the sluggish diffusion effect, and the "cocktail" effect, all of which are pivotal to structure-property studies in this field (Miracle and Senkov, 2017a). HEAs are defined from a signature concept, the high-entropy effect, which highlights that when five or more elements are combined they may favor forming of a solid solution over an intermetallic compound (Yeh et al., 2004).

For our view, the most unique structural character of HEAs is the antisite disordering of atomic types within an ordered crystal. This character could be extended to compounds and other applications. Rost et al. have synthesized rock-salt $(NiCoCuZnMg)O_x$ solid solution oxide (Rost et al., 2015) and these oxides are named as high-entropy oxides (HEOs) because they are also stabilized by high configurational entropy (Batchelor et al., 2019; Yan and Zhang, 2020). Up to now, numerous functional HEOs, high-entropy metallic glass (HEMGs) nanoparticles (NPs) (Glasscott et al., 2019), high-entropy borides (HEBs) (Gild et al., 2016), high-entropy sulfides (HESs) (Zhang et al., 2018b), high-entropy carbides (HECs) (Sarker et al., 2018), and high-entropy nitrides (HENs) (Jin et al., 2018) have also been developed. High-entropy materials (HEMs) including above compounds, are defined as any solid solution materials that consist of quasi-equimolar multicomponent (Dai, 2020). Recent works show that HEMs can be utilized for various energy-related applications, as catalysts for ammonia oxidation and decomposition (Xie et al., 2019; Yao et al., 2018); as electrocatalysts for oxidation (methanol [Wang et al., 2014]), carbon monoxide [Chen et al., 2018a; Dai, 2020]), evolution (oxygen [Qiu et al., 2019a], hydrogen [Zhang et al., 2018a]), reduction (carbon dioxide [Nellaiappan et al., 2020], oxygen [Löffler et al., 2018]), and degradation (azo dye [Lv et al., 2016]); as electrode for batteries (Dragoe and Bérardan, 2019; Oses et al., 2020); as hydrogen storage (Shen et al., 2019); as supercapacitors (Kong et al., 2019); etc. The structural tunability of HEMs provides them a great possibility for energy-related applications. For example, the large number of atomic sites on the surface of HEMs provides huge opportunity to tune the surface electronic structures, adsorption energies, and then the

[1]Shaanxi Materials Analysis and Research Center, School of Materials Science and Engineering, Northwestern Polytechnical University, Xi'an 710072, P. R. China

[2]Beijing National Laboratory for Condensed Matter Physics, Institute of Physics, Chinese Academy of Sciences, Beijing 100190, China

*Correspondence: msfu@nwpu.edu.cn (M.F.), maxiaonpu@nwpu.edu.cn (X.M.), dongsu@iphy.ac.cn (D.S.)

https://doi.org/10.1016/j.isci.2021.102177

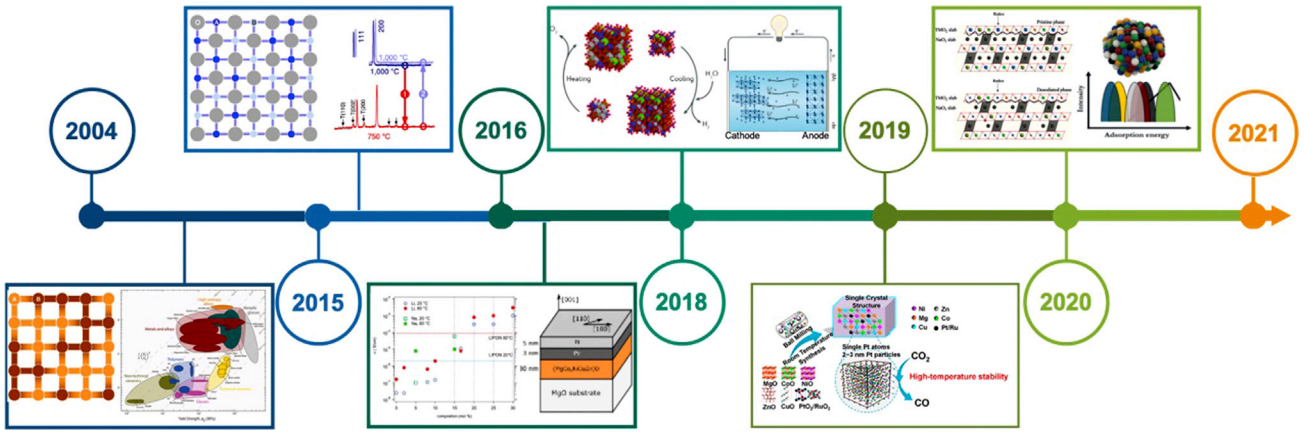

Figure 1. Roadmap of HEMs for recent energy-related applications

Before 2015, HEMs were mainly used as structural materials (Reproduced with permission from Gludovatz et al., 2014. Copyright © 2014, American Association for the Advancement of Science). Rost et al. discovered the entropy-stabilized oxides and named them as HEOs (Reproduced with permission from Rost et al., 2015. Copyright © 2015, Springer Nature). Then many other HEMs have been synthesized and utilized in solid electrolyte (Reproduced with permission from Bérardan et al., 2016a, 2016b. Copyright © 2016, The Royal Society of Chemistry), exchange coupling (Reproduced with permission from Meisenheimer et al., 2017. Copyright © 2017, Springer Nature), water decomposition (Reproduced with permission from Zhai et al., 2018. Copyright © 2018, The Royal Society of Chemistry), Li-ion battery (Reproduced with permission Wang et al., 2019. Copyright © 2019, Elsevier), COOR/CO_2RR catalysts (Reproduced with permission from Chen et al., 2019a. Copyright © 2019, American Chemical Society), and Na-ion battery (Reproduced with permission from Zhao et al., 2020a. Copyright © 2020, Wiley-VCH). Simultaneously, predictive models have been developed to guide the development of HEMs (Reproduced with permission from Löffler et al., 2020. Copyright © 2020, Wiley-VCH).

catalytic performances. HEMs for energy-related applications are usually in the form of nanoporous alloys or NPs to maximize their surface areas to prompt the reaction kinetics. Nanosized HEMs can be synthesized with wet-chemistry (solvothermal, ultrasonicated-assisted wet-chemistry, sol-gel auto-combustion, etc.), pulsed laser deposition (PLD), electrodeposition, carbothermal shock (CTS) methods, and so on, where processing temperature, heating, and cooling rates are key factors to form stable nanosized HEMs. In addition to thermodynamic stability, the uniform configuration of elements with different sizes through a single-phase solid solution also leads to severe lattice distortion, which then increases the activation barrier of diffusion (the sluggish diffusion effect) and improves kinetic stability (Usharani et al., 2020). The applications of HEMs for catalysis or energy storage have been investigated for less than one decade, and lots of explorations are needed for understanding well their structure-performance correlations.

In this work, we summarize the research progress of energy-related applications of HEMs. After a survey on the syntheses of HEMs, we introduce the structure and theory of HEMs and then the applications of nanosized HEMs, correlating with their structures, as shown in the roadmap of Figure 1. To keep the article brief, we skip the background knowledge of each application and focus on the structure-performance correlations of HEMs. In the last section, we present our perspectives on the challenges and future research opportunities.

SYNTHESES AND STRUCTURES

There are many physical or chemical synthetic routes being developed in the past 20 years to fabricate HEMs (Amiri and Shahbazian-Yassar, 2021; Tomboc et al., 2020; Xin et al., 2020). In the following discussion, we will briefly introduce separately the synthetic approaches of HEAs, HEOs, and other HEMs, correlating to their structural features.

Syntheses and structures of HEAs

Syntheses of HEAs

For energy-related applications, HEAs usually adopt nanostructures as nanoporous or NPs to maximize the surface area. Dealloying of bulk alloy is a common method to fabricate nanoporous HEA (such as AlMoCuPdAu, AlMnCoIrMo, AlNiCuPtPdAu, etc.) with enhanced surface area and uniform pore structures, ensuring high catalytic activity (Qiu et al., 2019b). Wet-chemistry is the general method to fabricate NPs through reduction of metallic precursors in solution. The general solution-based common chemical synthesis might

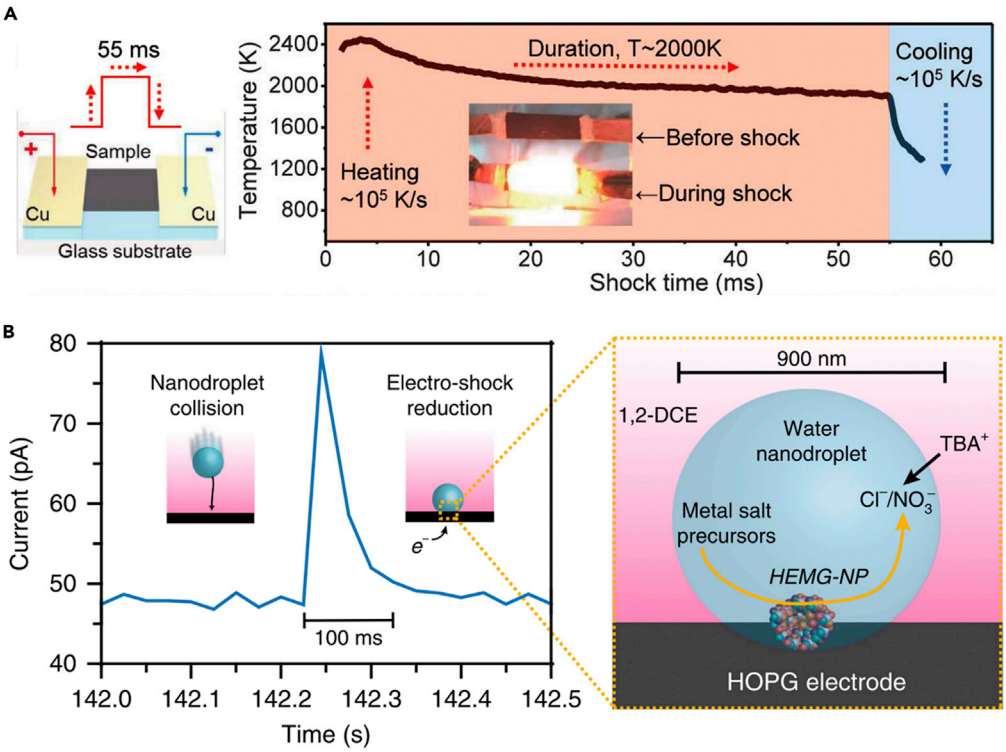

Figure 2. Syntheses of nanosized HEMs

(A) Carbothermal synthesis of HEA-NPs on carbon supports. Reproduced with permission from Yao et al. (2018). Copyright © 2018, American Association for the Advancement of Science.

(B) Nanodroplet-mediated electrodeposition synthesis controlling nanoparticle stoichiometry and microstructure. Reproduced with permission from Glasscott et al. (2019). Copyright © 2019, Springer Nature.

not be adequate for obtaining homogeneous nano-HEA with multi-components, and often severe decomposition or shock syntheses or reduction reactions are required (Bondesgaard et al., 2019). Liu et al. take advantage of ultrasonication to develop a facile ultrasonication-assisted wet-chemistry for preparing HEA NPs. The local temperature of the ultrasonication cavities is supposed to exceed extremely high temperature up to ~ 5,000°C, directly accelerating the metallic ions reduction to form entropy-maximized state, facilitating the formation of HEAs (Liu et al., 2019b).

In another case, Yao et al. developed the CTS method to prepare multicomponent HEA NPs. Precursor of metal salt mixtures was thermally shocked at ~ 2,000 K within 55 ms (as shown in Figure 2A), alloying up to eight dissimilar elements into single-phase solid-solution NPs (PtPdCoNiFeCuAuSn, etc.) loaded onto carbon support. This method can synthesize a wide range of multicomponent NPs with desired compositions and proper sizes by controlling the CTS parameters as well as supports, which may be a general route toward high performance and cost-effective catalysts (Yao et al., 2018). However, productivity of HEA NPs via CTS is very low. Future work to enhance the productivity for industrial applications is needed. Furthermore, Gao et al. developed a fast-moving bed pyrolysis (FMBP) method to prepare HEAs with diverse supports. Mixed metal precursors were rapidly heated to ~ 923 K (higher than their pyrolysis temperature) within 5 s. With this strategy, quinary FeCoPdIrPt, senary AuPdPtCuNiSn, octonary AuIrPdPtCoCuNiSn, and denary AuIrPdPtRhCoCuMnNiSn HEA NPs are successfully synthesized, exhibiting high mass activity and stability (Gao et al., 2020).

Table 1 has summarized the methods for preparing HEAs. For example, solvothermal (Bondesgaard et al., 2019), co-sputtering (Löffler et al., 2018), and deposition (Glasscott et al., 2019) have also been successfully developed to prepare HEA NPs. Electrodeposition can be used to produce multi-component HEMGs as PtCoFeLaNi, by confining multiple metal salt precursors to water nanodroplets emulsified in dichloroethane within 100 ms electroshock as shown in Figure 2B (Glasscott et al., 2019). The contents of

Table 1. Synthesis, structure, and application of HEMs

Applications	Composition	Structure	Form	Synthesis	References
Ammonia oxidation	PtPdRhRuCe, PtCoNiFeCuAu, PtPdCoNiCuAu, PtPdCoNiFeCuAuSn	fcc	Nanoparticle	Carbothermal shock	(Yao et al., 2018)
Ammonia decomposition	$Co_xMo_yFe_{10}Ni_{10}Cu_{10}$ (x + y = 70)	fcc	Nanoparticle	Carbothermal shock	(Xie et al., 2019)
HER	CoFeLaNiPt	fcc	Nanoparticle	Nanodroplet-mediated electrodeposition	(Glasscott et al., 2019)
	PtAuPdRhRu	fcc	Nanoparticle	Ultrasonication	(Liu et al., 2019b)
	IrPdPtRhRu	fcc	Nanoparticle	Facile one-pot polyol synthesis	(Wu et al., 2020a)
	AlMoCuPdAu	fcc	Nanoporous alloy	Dealloying	(Qiu et al., 2019b)
	FeCoPdIrPt	fcc	Nanoparticle	Fast-moving bed pyrolysis	(Gao et al., 2020)
	$Cr_{15}Fe_{20}Co_{35}Ni_{20}Mo_{10}$	fcc	Bulk	Arc-melting	(Zhang et al., 2018a)
	$(FeMnCoNi)_xO$	Rock-salt + spinel	Micro-powders	Sol-gel and solid-state sintered	(Zhai et al., 2018)
	$(CrMnFeCoNi)_xP$	Hexagonal	Nanosheet	Eutectic solvent method	(Zhao et al., 2020b)
OER	CrMnFeCoNi	fcc	Nanoparticle	Laser	(Waag et al., 2019)
	AlMoCuPdAu	fcc	Nanoporous alloy	Dealloying	(Qiu et al., 2019b)
	CoFeLaNiPt	fcc	Nanoparticle	Nanodroplet-mediated electrodeposition	(Glasscott et al., 2019)
	AlMoCoIrMo	fcc	Nanoporous alloy	Dealloying	(Jin et al., 2019)
	$(FeMnCoNi)O_x$ (x ~ 1.2)	Rock-salt + spinel	Micro-powders	Sol-gel and solid-state sintered	(Zhai et al., 2018)
	FeMnCoNi (+$(FeMnCoNi)O_x$)	fcc	Micro-powders	Mechanical alloying	(Dai et al., 2019)
	$(CrMnFeCoNi)_xP$	Hexagonal	Nanosheet	Eutectic solvent method	(Zhao et al., 2020b)
	$K(MgMnFeCoNi)F_3$, $K(MgMnCoNiZn)F_3$	Perovskite	Nanoparticle	Boiled solution by combining a hydrothermal method with mechanochemistry	(Wang et al., 2020b)
ORR	CrMnFeCoNiNb, CrMnFeCoNiMo	fcc	Nanoparticle	Combinatorial co-sputtering	(Löffler et al., 2018)
	AlNiCuPtPdAu	fcc	Nanoporous	Dealloying	(Qiu et al., 2019b)
	Al-Cu-Ni-Pt-Mn	fcc	Nanoporous alloy	Selective dealloying	(Li et al., 2020b)
COOR	AlMoCuPdAu	fcc	Nanoporous alloy	Dealloying	(Qiu et al., 2019b)
	$PtNiMgCuZnCoO_x$	Rock-salt	Micro-powder	Solid-state sintered	(Chen et al., 2018a)
	$Ru/BaSrBi(ZrHfTiFe)O_3$	Perovskite	Nanoparticle	Sonochemical-based synthesis	(Okejiri et al., 2020)
	$(CuNiFeCoMg)O_x-Al_2O_3$	Rock-salt	Mesoporous	Mechanochemical solid state	(Zhang et al., 2019b)
CO_2RR	AuAgPtPdCu	fcc	Nanocrystalline	Cast cum cryo-milling	(Nellaiappan et al., 2020)
	Pt/Ru-(NiMgCuZnCo)O	fcc	Micro-powder	Mechanochemical	(Chen et al., 2019a)
Methanol oxidation reaction	$Ir_{0.19}Os_{0.22}Re_{0.21}Rh_{0.20}Ru_{0.19}$	hcp	Bulk	Thermal decomposition	(Yusenko et al., 2017)
	AlMoCuPdAu	fcc	Nanoporous alloy	Dealloying	(Qiu et al., 2019b)
Ethanol oxidation reaction	RuRhPdOsIrPt	fcc	Nanoparticle	Wet-chemistry	(Wu et al., 2020b)

(*Continued on next page*)

Table 1. *Continued*

Applications	Composition	Structure	Form	Synthesis	References
Water oxidation	$(Co,Cu,Fe,Mn,Ni)_3O_4$	Spinel	Nanoparticle	Facile methodology	(Wang et al., 2019)
Oxidation of aromatic alcohols	$(Mg_{0.2}Co_{0.2}Ni_{0.2}Cu_{0.2}Zn_{0.2})O$	Rock-salt	Holey lamellar	Anchoring-merging process	(Feng et al., 2020a)
Li-ion battery	$(Co_{0.2}Cu_{0.2}Mg_{0.2}Ni_{0.2}Zn_{0.2})O$	Rock-salt	Nanoparticle	Flame spray pyrolysis, Nebulized spray pyrolysis, Reverse co-precipitation	(Sarkar et al., 2018)
	$(Co_{0.2}Cu_{0.2}Mg_{0.2}Ni_{0.2}Zn_{0.2})O$	Rock-salt	Nanoparticle	Solid-state sintered & ball milling	(Chen et al., 2019b)
	$(MgCoNiZn)_{1-x}Li_xO$ (x = 0.05, 0.15, 0.25, and 0.35)	Rock-salt	Bulk	Solid-state sintered	(Lökçü et al., 2020)
	$(Mg_{0.2}Ti_{0.2}Zn_{0.2}Cu_{0.2}Fe_{0.2})_3O_4$	Spinel	Powder	Solid-state sintered	(Chen et al., 2020b)
	$(Mg,Ti,Zn,Cu,Fe)_3O_4$	Spinel	Nanoparticle	Surfactant-assisted hydrothermal	(Nguyen et al., 2020)
	$[(Bi,NA)_{1/5}(La,Li)_{1/5}(Ce,K)_{1/5}Ca_{1/5}Sr_{1/5}]TiO_3$	Perovskite	Bulk	Solid-state sintered	(Yan et al., 2020)
Na-ion battery	$NaNi_{0.12}Cu_{0.12}Mg_{0.12}Fe_{0.15}Co_{0.15}Mn_{0.1}Ti_{0.1}Sn_{0.1}Sb_{0.04}O_2$	O3	Micro-powder	Solid-state sintered	(Zhao et al., 2020a)
Solid oxide fuel cell	$La_{1-x}Sr_x(CoCrFeMnNi)O_{3-\delta}$ (x = 0, 0.1, 0.2, 0.3)	Perovskite	Bulk	Sol-gel & solid-state sintered	(Dąbrowa et al., 2020)
Solid-state electrolytes	$(MgCoNiCuZn)_{1-x-y}Ga_yA_xO$ ($A = Li^+, Na^+, K^+$)	Rock-salt	Bulk	Solid-state sintered	(Bérardan et al., 2016b)
Semiconductor	$(Cr,Fe,Mg,Mn,Ni)_3O_4$	Spinel	Bulk	Solid-state sintered	(Stygar et al., 2020)
Hydrogen storage	TiZrHfMoNb	bcc	Micro-powder	Arc-melting & grinding	(Shen et al., 2019)
Supercapacitors	FeNiCoMnMg	fcc	Nanoparticle	Carbothermal shock	(Xu et al., 2020)
	AlCoCrFeNi	fcc	Nanoporous alloy	Selective dissolution	(Kong et al., 2019)
	(TiNbTaZrHf)C	fcc	Nanoparticle	Facile electrochemical	(Sure et al., 2020)
	(CrMoVZrNb)N	fcc	Micro-powder	Mechanochemical-assisted soft urea strategy	(Jin et al., 2018)
Colossal dielectric	$(Mg,Co,Ni,Cu,Zn)_{1-x}Li_xO$	Rock-salt	Bulk	Solid-state sintered	(Bérardan et al., 2016a)
Exchange coupling	$(Mg_{0.25(1-x)}Co_xNi_{0.25(1-x)}Cu_{0.25(1-x)}Zn_{0.25(1-x)})O$	Rock-salt	Film	Solid-state sintered & pulsed laser deposition	(Meisenheimer et al., 2017)
Wear	(Al0.17Ti0.41V0.14Cr0.04Nb0.24)N, (Al0.31Ti0.34V0.12Cr0.06Nb0.17)N	fcc	Film	Cathodic arc deposition	(Yalamanchili et al., 2017)
High-temperature oxidation resistance	$(Hf_{0.2}Zr_{0.2}Ta_{0.2}Mo_{0.2}Ti_{0.2})B_2$	Hexagonal layered	Bulk	Spark plasma sintering	(Gild et al., 2016)

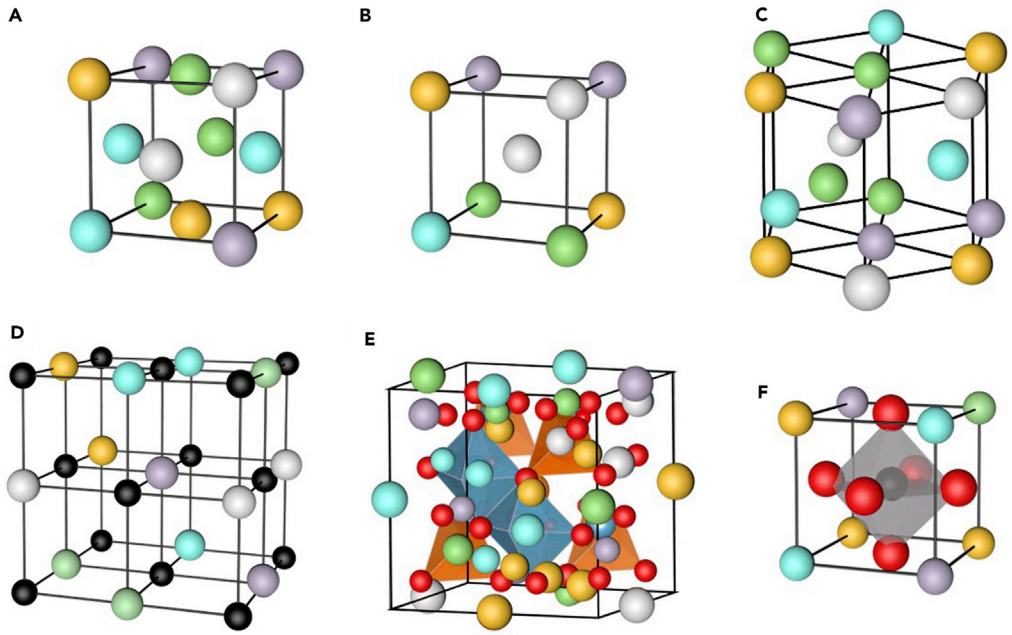

Figure 3. Typical structures of HEAs, HEOs, and other HEMs

(A) fcc lattice structure, (B) bcc lattice structure, (C) hexagonal crystal structure, (D) rock-salt structure, (E) spinel structure, and (F) perovskite structure.

nanodroplet are entirely reduced during collision, enabling disordered co-deposition of different metal precursors. CrMnFeCoNi NPs with an averaged diameter of 1.7 nm were synthesized by combinatorial co-sputtering into the [Bmim]-[Tf_2N] (Löffler et al., 2018). Bondesgaard et al. developed a general solvothermal synthesis method for PtPdIrRhRu HEA nanocatalysts (Bondesgaard et al., 2019).

It was proposed that the key factor to synthesize HEA NPs is to control the cooling rate (Yao et al., 2018). A proper cooling rate, ranging from several seconds to several minutes depending on the system or synthesis method, facilitated the formation of single-phase solid solutions with certain crystal structures, enabling HEA structures. However, we believe that in most cases, reduction of all components at the same time in solutions is a key issue instead of the cooling rate, which is evidenced by the work by Gao et al. and Wu et al., showing that a slow cooling rate may also prompt the formation of HEAs (Gao et al., 2020; Wu et al., 2020a).

Structure of HEAs

HEAs can have cubic crystal structure with fcc lattice (Figure 3A) and bcc lattice (Figure 3B), hexagonal crystal structure (Figure 3C), and other structures (Ostovari Moghaddam and Trofimov, 2021; Yan and Zhang, 2020; Ye et al., 2016). Fcc lattice is by far the most extensively investigated structure of HEAs (George et al., 2019; Gorsse et al., 2017; Li et al., 2019; Miracle and Senkov, 2017b). For energy-related applications, nano-HEAs such as CoMoFeNiCu and CoFeLaNiPt with fcc lattice have a lattice parameter of $a \approx 3.6$ Å. HEAs containing heavy hcp metals (mainly Os, Re, Ru, and Zr) could form hcp structure. Yusenko et al. synthesized $Ir_{0.19}Os_{0.22}Re_{0.21}Rh_{0.20}Ru_{0.19}$ HEA with space group $P6_3/mmc$ and lattice parameters $a = 2.728$ Å and $c = 4.338$ Å (Yusenko et al., 2017). Reports on the syntheses and structures of HEA NPs with different crystal structures are summarized in Table 2. The fundamental correlations between the compositions and phases, e.g., a phase diagram for HEAs, are not clear at present, which is highly needed in future.

Syntheses and structures of HEOs

Syntheses of HEOs

High-entropy compounds can be synthesized from binary metal compound precursors. For HEO in bulk form, traditional methods including solid-state sintering (Rost et al., 2015), spark plasma sintering (Biesuz et al., 2019; Gild et al., 2019), and reactive flash sintering (Liu et al., 2020; Wang et al., 2020a) have been

Table 2. Synthesis and structure of HEA NPs

Structure	Composition	Synthetic method	Form	Catalytic application	References
fcc	PtRuCuOsIr	Mechanical alloying (chemical dealloying)	Nanoporous	Methanol oxidation & oxygen reduction	(Chen et al., 2015)
	AlNiCuPtPdAu AlNiCuPtPdAuCoFe AlNiCuMoCoFe	Arc-melting & dealloying		CO oxidation	(Qiu et al., 2019b)
	AlNiCoIrMe (Me: Mo, Cr, Cu, Nb, V)	Arc-melting & dealloying		Oxygen evolution reaction	(Jin et al., 2019)
	AlNiCoFeMe (Me: Mo, Cr, V, Nb)	Arc-melting & dealloying		Oxygen evolution reaction	(Qiu et al., 2019a)
	AlCuNiPtMe (Me: Mn, Co, Mo, Pd, Au)	Arc-melting & dealloying		Oxygen reduction reaction	(Li et al., 2020b)
	MnFeCoNi	Ball milling	Powder	Oxygen evolution reaction	(Dai et al., 2019)
	CuAgAuPtPd	Arc-melting & cryogrinding		Formic acid & methanol electro-oxidation	(Katiyar et al., 2020)
	AuAgPtPdCu	Arc-melting & cryogrinding		CO_2 & CO reduction reactions	(Nellaiappan et al., 2020)
	CoCrFeMnNi	Mechanical alloying (ball milling)		Degrading azo dye solutions	(Hu et al., 2019)
	CoMoFeNiCu RuRhCoNiIr	Carbothermal shock	Nanoparticle	NH_3 decomposition	(Xie et al., 2019; Yao et al., 2020b)
	PtPdRhRuCe	Carbothermal shock		NH_3 oxidation	(Yao et al., 2018)
	RuIrCeNiWCuCrCo	Carbothermal shock		Oxygen electrocatalysis	(Lacey et al., 2019)
	PtPdRhNi PtPdFeCoNi	Carbothermal shock		Electrocatalysts	(Yao et al., 2020a)
	NiCoCuFePt	Aerosol synthesis		–	(Yang et al., 2020)
	IrOsReRhRu	Thermal decomposition		Methanol oxidation	(Yusenko et al., 2017)
	CrMnFeCoNi	Combinatorial co-sputtering		Oxygen reduction reaction	(Löffler et al., 2018)
	PtAuPdRh PtAuPdRhRu	Ultrasonication-assisted wet chemistry		Hydrogen evolution reaction	(Liu et al., 2019b)
	MnFeCoNiCu	MOF-template method		Oxygen evolution reaction	(Huang et al., 2020)
	IrPdPtRhRu	One-pot polyol process		Hydrogen evolution reaction	(Wu et al., 2020a)
	CoCrCuNiAl	Sol-gel autocombustion synthesis		Superparamagnetic behavior	(Niu et al., 2017)
	CoCrFeMnNi	Laser ablation		Oxygen evolution reaction	(Waag et al., 2019)
	PtIrPdRhRu	Auto-catalytic formation		–	(Broge et al., 2020)
	CuPdSnPtAu NiCuPdSnAuPt MnCoNiCuRhPdSnIrPtAu, etc.	Fast moving bed pyrolysis		Hydrogen evolution reaction	(Gao et al., 2020)
	PtNiFeCoCu	One-pot oil phase synthesis method		Hydrogen evolution reaction & methanol oxidation reaction	(Li et al., 2020a)
	CuPdPtAu	Electrochemical synthesis		Oxygen reduction reaction	(Park and Ahn, 2020)
	IrPdPtRhRu	One-pot oil phase synthesis method		Ethanol oxidation reaction	(Wu et al., 2020b)
	RuFeCoNiCu	One-pot oil phase synthesis method		Electrocatalytic nitrogen reduction reaction	(Zhang et al., 2020)
	AuAgCuPd AuNiAgCrCoMo, etc.	Oscillatory spark method		Ethanol oxidation reaction, ethanol oxidation reaction, & formic acid oxidation reaction	(Feng et al., 2020b)
	PtFeCoNiCuAg	Radio-frequency sputter deposition		Methanol oxidation reaction	(Tsai et al., 2009)

(*Continued on next page*)

Table 2. ***Continued***

Structure	Composition	Synthetic method	Form	Catalytic application	References
bcc	AlCoCrTiZn AlCoCrFeNi	Mechanical alloying (ball milling)	Powder	Degrading azo dye solutions	(Hu et al., 2019)
	CoCrCuNiAl	Sol-gel autocombustion synthesis	Nanoparticle	Superparamagnetic behavior	(Niu et al., 2017)
hcp	IrOsReRhRu	Thermal decomposition	Nanoparticle	Methanol oxidation	(Yusenko et al., 2017)
Amorphous	CoFeLaNiPt CoCrMnNiV CoFeLaMnNi	Nanodroplet-mediated electrodeposition	Nanoparticle	Oxygen reduction reaction & hydrogen evolution reaction	(Glasscott et al., 2019)

successfully developed. The sintering temperature and soaking time are key factors for the syntheses of bulk HEOs.

With proper solvent, heating/cooling rates, and reaction temperatures, shocking methods as CTS, FMBP, and pulsed laser deposition (PLD) might be adequate to fabricate HEO NPs from bulk HEOs similar with HEA. Films of $(Mg_{0.2(1-x)}Co_xNi_{0.2(1-x)}Cu_{0.2(1-x)}Zn_{0.2(1-x)})O$ (x = 0.2, 0.27, 0.33) were fabricated by solid-state sintering combined with PLD method (Meisenheimer et al., 2017). This method was also proved to be practicable in the fabrication of $(MgNiCoCuZnSc)_xO$ ($x \sim 0.167$) and $(LaPrNdSmEu)_{0.2}NiO_3$ (Kotsonis et al., 2018; Patel et al., 2020).

Wet-chemistry methods (Biesuz et al., 2018) such as solution combustion (Xiang et al., 2020), flame spray pyrolysis, nebulized spray pyrolysis (NSP), reverse co-precipitation (Sarkar et al., 2017), etc., have been successfully applied to the fabrication of $(CoCuMgNiZn)O_x$ HEO NPs. Among these methods, the NSP method might have broad prospect because it can directly synthesize nanocrystalline single phase. Wang et al. have used $Co_{0.2}Cu_{0.2}Mg_{0.2}Ni_{0.2}Zn_{0.2}O$ as the precursor and LiF or NaCl as the reactant to prepare Li-containing entropy-stabilized oxyfluoride (HEOF) of $Li_x(Co_{0.2}Cu_{0.2}Mg_{0.2}Ni_{0.2}Zn_{0.2})OF_x$ (Wang et al., 2019b).

Structure of HEOs

HEOs with fcc lattice constitute a large portion of energy-related applications such as catalysis and battery electrode materials. Among fcc structures, rock-salt HEO of $(MgCoNiCuZn)O_x$ was synthesized by Rost et al. (Figure 3D) (Rost et al., 2015). Extended X-ray absorption fine structure and scanning transmission electron microscopy (STEM) analyses reveal that the first-near-neighbor cation-to-anion distances of this compound are identical (Rost et al., 2017). With a substitution of Li^+ up to 16.6%, this HEO still keeps its rock-salt structure, shedding potential for energy-storage applications (Bérardan et al., 2016b). Recently, Jimenez-Segura et al. reported that this kind of rock-salt HEO exhibits a long-range magnetic order coexisted with the component disorder, and Zhang et al. found that the magnetic order in this HEO might correlate with Cu^{2+} Jahn-Teller distortions through neutron diffraction (Jimenez-Segura et al., 2019; Zhang et al., 2019a).

Berardan et al. studied the distortion and atomic disordering of this HEO using X-band electron paramagnetic resonance spectroscopy. They proposed that post-annealing treatment can adjust the local environment of Cu^{2+}, from octahedral in air-quenched Cu-sub-stoichiometric samples to rhombic in Cu-enriched HEOs, and then adjust the Jahn-Teller distortion and the dielectric property (Berardan et al., 2017). The results agreed with the density functional theory (DFT) calculations by Rák et al. Splitting of the Cu d-states near the Fermi level after relaxation suggests a Jahn-Teller distortion involving O-atom, which offers new possibilities of tuning the dielectric, magnetic, superconductivity, etc., properties of HEOs (Rák et al., 2018).

HEOs composed of multicomponent rare earth elements as $(Ce,La,Pr,Sm,Y)_2O_{3+x}$ synthesized by NSP method have CaF_2-type structures. Interestingly, Djenadic et al. suggested that they cannot maintain single phase without Ce (such as (Ga, La, Nd, Pr, Sm, Y)O) (Djenadic et al., 2017). In addition, Chen et al. found that $(HfZrCeTiSn)O_2$ with CaF_2 structure exhibits a single phase at high temperature and multiphase at low temperature, which is believed as an evidence of entropy stabilization (Chen et al., 2018b). It seems that not only the entropy effect but also the compositions affect the structural stabilization of HEOs in addition to the synthesis procedure and the crystal size.

Spinel HEOs (as shown in Figure 3E) such as $(Cr,Fe,Mg,Mn,Ni)_3O_4$ and (Co,Mg,Mn,Ni,Zn) Al,Co,Cr,Fe, $Mn)_2O_4$ with a space group of Fd3m can be synthesized by solid-state sintering (Dąbrowa et al., 2018; Fracchia et al., 2020b; Stygar et al., 2020). Based on $NiFe_2O_4$, $(Co_{0.2}Cr_{0.2}Fe_{0.2}Mn_{0.2}Ni_{0.2})Fe_{1.9}(Dy_{0.02}Er_{0.02}Gd_{0.02}Ho_{0.02}Tb_{0.02})O_4$ were synthesized by sol-gel method enhanced by entropy stabilization (Parida et al., 2020). $(Cr_{0.2}Fe_{0.2}Mn_{0.2}Ni_{0.2}Zn_{0.2})_3O_4$ nanocrystalline spinel powders have been synthesized by solution combustion with good magnetic properties (Mao et al., 2020).

HEMs with perovskite structure (ABX_3) have fruitful physical properties with a broad range of energy-related applications, which contains 12-fold coordinated A-site cations, 6-fold coordinated B-site cations, and X anion octahedra (Figure 3F). To form a single high-entropy perovskite phase, the "tolerance factor" of *t* has to be close to unity ($t \approx 1.0$) (Patel et al., 2020).

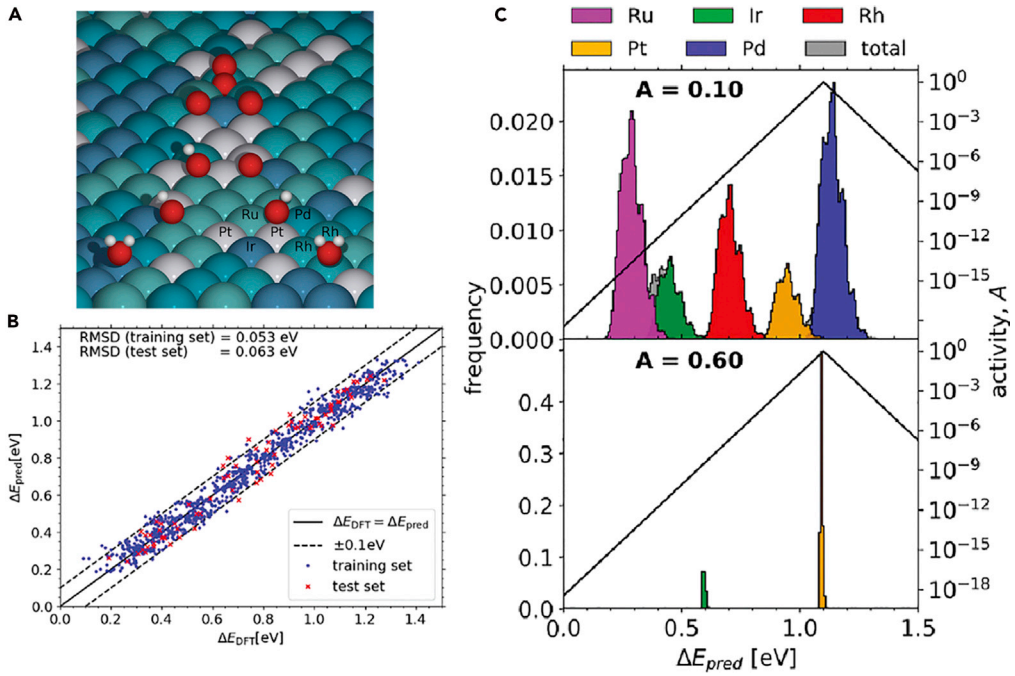

Figure 4. Predictive model of HEA for electrocatalysis

(A) Schematic of oxygen reduction reaction on the surface of IrPdPtRhRu HEA.

(B) Comparison of *OH adsorption energies machine learned on 871 samples (blue dots) and DFT calculation tested on 76 samples (red crosses).

(C) Distribution of adsorption energies for predicted $Ir_{10.2}Pd_{32.0}Pt_{9.30}Rh_{19.6}Ru_{28.9}$ (upper) and $Ir_{17.5}Pt_{82.5}$ (lower), which show excellent activity for ORR. Reproduced with permission from Batchelor et al. (2019). Copyright © 2018, Elsevier.

Syntheses and structures of other HEMs

Methods similar to preparation of HEOs can be used to synthesize other high-entropy compounds. Sure et al. synthesized nanoscale HEC of $(TiNbTaZrHf)C_x$ with fcc lattice via a facile electrochemical process (Sure et al., 2020). Liu et al. developed a facile borothermal reduction method to produce HEB of $(Hf_{0.2}Zr_{0.2}Ta_{0.2}Nb_{0.2}Ti_{0.2})B_2$ in hexagonal crystal structure with average particle size of 310 nm (Liu et al., 2019a). Similar method as molten salt-mediated magnesiothermic reduction can prepare $(Zr_{0.25}Ta_{0.25}Nb_{0.25}Ti_{0.25})B_2$ HEB NPs with size of 28 – 56 nm (Ye et al., 2020).

Table 1 summarizes the synthetic methods for the construction of efficient nano-HEMs with well-controlled composition, size, and uniformity, including both top-down and bottom-up methods. For the top-down methods, proper cooling/heating rate and appropriate duration time are required to be well controlled to prepare HEMs with adequate size. For the bottom-up methods based on wet-chemistry, low cost and high productivity are key factors for industrial production. Here we listed the reported structures of HEMs. More explorations will be emerging as according to our view there is no fundamental rule excluding HEMs from other structures.

Surface structure and activity

HEMs provide a large amount of surface sites with different atomic environments associated with various adsorption energies. For example, heterogeneous catalysts may speed up chemical reactions at active sites on the surface. HEM-based catalysts provide plentiful possible combinations of surface structure (then electronic structure) and the opportunity to achieve optimized catalytic performances. Batchelor et al. used theory to understand the activity of HEA catalysts and optimize the use of IrPdPtRhRu HEAs for catalyzing the oxygen reduction reaction (ORR). Figure 4A shows a schematic of *OH adsorbed on (111) plane of IrPdPtRhRu using nearest neighbor model. Through the DFT calculations of *OH adsorption energies on surface sites (Figure 4B), they predicted that near-continuous adsorption energies can be spanned out by tuning surface configurations (Batchelor et al., 2019; Pedersen et al., 2020). Then it is possible to engineer the surface structure to maximize the catalytic activity with peak value of adsorption

energies (Figure 4C). The IrPdPtRhRu HEA and binary IrPt alloy identified in this study show significant activity enhancement over Pt(111) (Wang and Xin, 2019). Besides the surface structure, the variety of local electronic structure will intrinsically affect the other basic properties of HEMs, such as ionic/electronic conductivity, thermal conductivity, charge distribution magnetic properties, and dielectric properties. These properties may affect their catalytic properties through mass transfer, charge transfer, etc.

The structure of HEMs is believed to be stabilized by the high level of atomic disorder throughout the simple crystal structure and maximized entropy. Ratio of formation enthalpy to entropy and the differences in atomic radii are the core factors that affect their stability (Sarkar et al., 2020a). It is not clear if the surface structures of HEMs can also be preserved at working conditions.

Structural characterizations of HEMs

The structure of HEMs is featured with a single solid solution where the atoms disorderly distributed in lattice. The structural characterization demands the crystallography characterization and the chemical configuration including chemical composition and distribution. The former one can be realized with analytic methods such as X-ray diffraction (XRD), selected area electron diffraction (SAED), electron back-scattered diffraction, and high-resolution transmission electron microscopy (HRTEM) (Bondesgaard et al., 2019). The last of these is normally done with energy-dispersive spectrometry (EDS), wavelength-dispersive spectrometry, X-ray absorption spectroscopy (XAS), electron energy loss spectrometry, atomic probe tomography (APT), and inductively coupled plasma-optical emission spectrometry (Xie et al., 2019). In addition, scanning electron microscopy (SEM), atomic force microscopy, TEM, and high-angle annular dark-field (HAADF) STEM are useful for microstructure analysis (Liu et al., 2019b). HRTEM and high-resolution STEM have been used to clarify the atomic configuration uniformity (Gao et al., 2020). Hard X-ray can detect the electron structure and bond length of HEM (Sarkar et al., 2020b). The combination of the aforementioned methods may have advantages to reveal the local structure: for example, Ding et al. proposed that elements adopted greater aggregation with a wavelength of incipient concentration waves in CrFeCoNiPd bulk alloy, with the assistant of aberration-corrected TEM and EDS mapping (Ding et al., 2019).

APPLICATIONS

Catalysis

Ammonia oxidation

Yao et al. synthesized PtPdRhRuCe, PtCoNiFeCuAu, PtPdCoNiCuAu, and PtPdCoNiFeCuAuSn nanocrystals with fcc lattice via the CTS method. They found that PtPdRhRuCe NPs exhibits excellent activity for ammonia oxidation with $\sim$ 100% conversion and > 99% nitrogen oxide selectivity toward NO_x (NO + NO_2) (Figure 5A) (Yao et al., 2018). The enhanced catalytic selectivity is suggested due to the highly atomically homogeneous nature of the solid-solution NPs, compared with the lower activity of the phase separated heterostructures. In addition, PtPdRhRuCe NPs show no activity degradation owing to their high-entropy nature preventing phase separation or elemental segregation (as shown in Figure 5B).

Ammonia decomposition

Co-Mo nanoalloys show high activity for the reaction of ammonia decomposition. Xie et al. found that quinary CoMoFeNiCu NPs ($Co_xMo_yFe_{10}Ni_{10}Cu_{10}$ (x + y = 70)) on carbon nanofiber exhibit an even higher NH_3 conversion rate than either binary Co-Mo or Ru catalysts (Xie et al., 2019). The HEA-Co_xMo_y catalysts are stable and highly efficient for NH_3 decomposition, achieving a more than 20 times improvement versus Ru catalyst. It is well known that in a Co-rich system, the rate is limited by NH_3 activation, whereas in a Mo-rich system, the rate is limited by the *N desorption. Importantly, the catalytic activity of these HEA NPs is found regulated by the Co/Mo ratio (Figure 5C). Thus, their catalytic activities and catalytic kinetics exhibited a volcano-type profile described by the nitrogen adsorption energy (Figure 5D) (Xie et al., 2019). Guided by the DFT calculations, another quinary system, RuRhCoNiIr exhibits 5 times higher efficiency for NH_3 decomposition than the separated phases at 550 K. Similarly, its outstanding catalytic performance and high stability were attributed to the synergistic effect of the ultrafine size, the uniform dispersion, the multi-elemental composition, and the fcc lattice structure (Yao et al., 2020b).

Oxidation of aromatic alcohols

Feng et al. synthesized a holey lamellar HEO of $Co_{0.2}Ni_{0.2}Cu_{0.2}Mg_{0.2}Zn_{0.2}O$ with mesoporous structure by anchoring and merging. This compound has ultra-high catalytic activity for the solvent-free aerobic

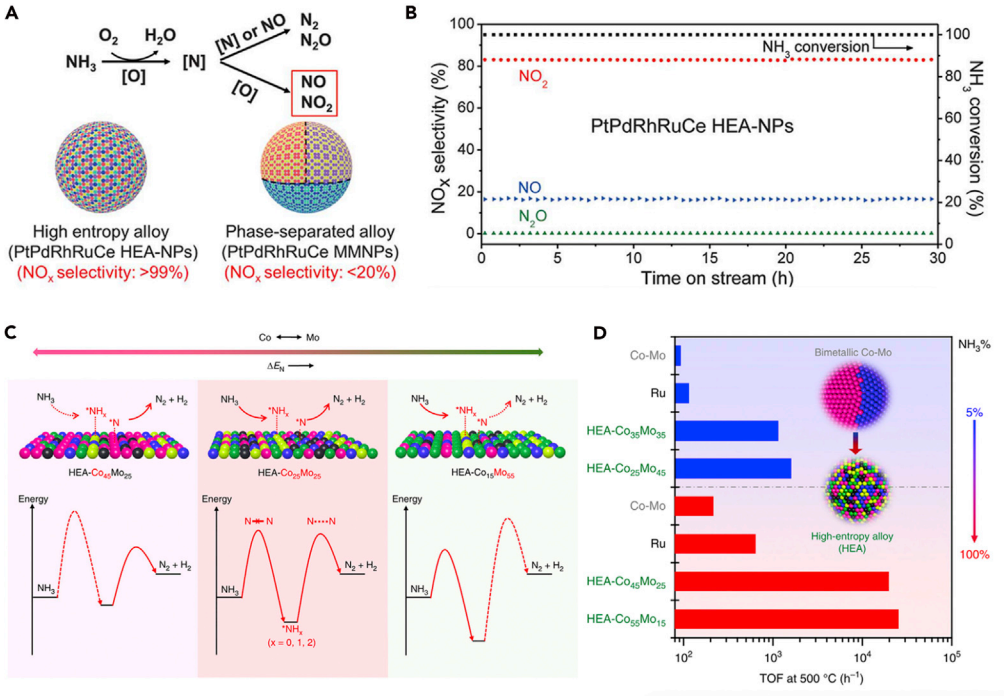

Figure 5. HEA NPs for ammonia oxidation and decomposition reactions

(A) Detailed steps of ammonia oxidation process over HEA NP catalysts highlighting how the apparent catalytic activity differences between the PtPdRhRuCe HEA NPs and phase-separated PtPdRhRuCe are due to different structure.

(B) Time-dependent catalytic performance with consideration of selectivity of PtPdRhRuCe HEA NPs at 700 °C. Reproduced with permission from Yao et al. (2018). Copyright © 2018, American Association for the Advancement of Science.

(C) Schematic of the rate-limiting factors in NH_3 decomposition over HEA NP catalysts.

(D) NH_3 decomposition efficiency in different systems. Reproduced with permission from Xie et al. (2019). Copyright © 2019, Springer Nature.

oxidation of benzyl alcohol, with 98% conversion achieved in only 2 h. It has been considered that the highly catalytic activity could be enhanced by abundant oxygen vacancies and holey lamellar framework in the HEO (Feng et al., 2020a). Understanding this example, it is clear that HEO catalysts show promise in a variety of catalytic reactions including many examples of thermocatalysis.

Electrocatalysis

Electrochemical devices for energy-related applications were normally utilized at relatively low temperature of ~ 80 °C and liquid environment. HEM catalysts have been developed for the following hydrogen evolution reaction (HER), oxygen evolution reaction (OER), ORR, CO/CO_2 reduction reaction (CORR/CO_2RR), CO oxidation reaction (COOR), methanol/ethanol oxidation reaction (MOR/EOR), etc. We introduced the representative works in following text.

Hydrogen evolution reaction

Normally HEAs show better corrosion resistance than normal alloys due to their locally disordered chemistry. Therefore, HEAs were considered as highly active and stable electrocatalysts for HER in both acidic and basic electrolytes. It is reported that the $Ni_{20}Fe_{20}Mo_{10}Co_{35}Cr_{15}$ catalyst has an overpotential of 107 mV in acidic solutions and 172 mV in the basic solution, respectively, showing much better activity than the dual-phase catalyst. This activity is even comparable to that of Pt sheet. The high HER activity of HEA is believed to be enhanced by their partially filled *d*-orbitals fitting for the gain and loss of electrons, promoting the adsorption of hydrogen (Zhang et al., 2018a). As shown in Figures 6A and 6B, the CoFeLaNiPt HEMGs can be electro synthesized with equimolar components by confining multiple metal salt precursors to water nanodroplets (Glasscott et al., 2019). This system shows a high HER overpotential of 555 ± 2 mV and a high OER overpotential of 377 ± 4 mV, respectively, benefitted from synergistic activity from Pt sites

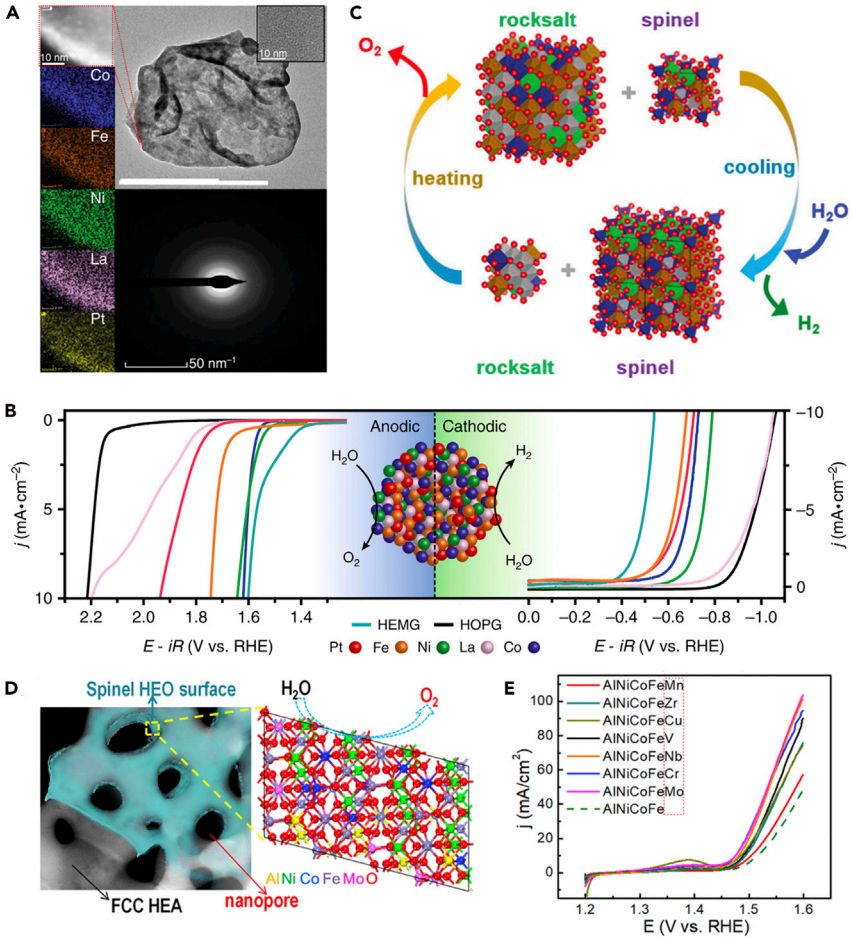

Figure 6. HEM electrocatalysts for HER and OER

(A) Elemental mappings and electron diffraction pattern show structural uniformity of CoFeNiLaPt HEMP NP.

(B) Electrocatalytic evaluation of a CoFeLaNiPt electrocatalyst. Reproduced with permission from Glasscott et al. (2019). Copyright © 2019, Springer Nature.

(C) Schematic of two-step thermochemical water splitting using a $(FeMnCoNi)_xO$ HEO. Reproduced with permission from Zhai et al. (2018). Copyright © 2018, The Royal Society of Chemistry.

(D) HAADF image and structure of nanoporous AlNiCoFeMo HEA covered with $(AlNiCoFeMo)_xO$ HEO surface.

(E) Linear scanning voltammetry curves showing the oxygen evolution activity on the different nanoporous HEAs and nanoporous AlNiCoFe. Reproduced with permission from Qiu et al. (2019a). Copyright © 2019, American Chemical Society.

and transition metal sites. Wu et al. also successfully synthesized a highly active RuRhPdIrPt HER catalyst. Hard X-ray photoelectron spectroscopy (XPS) analysis reveals that this kind of HEA has a broad and featureless valence band spectrum. The authors believe that the featureless XPS spectra imply random atomic configurations with a variety of local electronic structures and unique local density states in HEA, and different atomic configurations have distinct local electronic structures and spectra characteristics in general phases (Wu et al., 2020a).

In addition to HEA catalysts, Zhai et al. discovered HEO mixture of $(FeMgCoNi)O_x$ ($x \sim 1.2$) composed of rock-salt structure and spinel structure can thermochemically split water and produce H_2 and O_2 in a two-step cycle. During the reaction, the HEO mixture experiences a reversible phase swing between rock-salt and spinel phases (Figure 6C). The rock-salt oxide became thermally reduced at a higher temperature and released O_2, and then the reduced oxide cooled to a lower temperature and was oxidized by water to produce H_2 during thermochemical cycling. Interestingly, XAS analysis shows Fe component, the only redox-active species in the HEO. However, Fe ions in well-studied spinel ferrites are purely Fe^{3+}, which is believed

to have a larger redox capacity than a spinel/rock-salt two-phase oxide system where both Fe^{2+} and Fe^{3+} are present (Zhai et al., 2018). Furthermore, Zhao et al. prepared $(CrMnFeCoNi)_xP$ HEMP nanosheets with hexagonal crystal structure, which presents a current density of 10 mA/cm^2 at an overpotential of 136 mV for HER. The enhanced electrocatalytic activity might be benefited from the synergistic activity of the components (Zhao et al., 2020b).

Oxygen evolution reaction

Developed from NiFe or NiCoFe nano-alloys, nanoporous AlNiCoFeX (X = Mo, Nb, Cr) HEAs covered with a naturally oxidized surface exhibit low impedance resistance and excellent electrochemical durability as OER catalysts (Figure 6D). These catalysts were synthesized with chemical etching, a top-down strategy that is typically considered to be highly reproducible and applicable to the syntheses of other HEA catalysts. Cr, Nb, V, Zr, Mn, Cu, Mo, etc., have been added and formed nanoporous AlNiCoFeX HEAs, enhancing the OER activity. Among them, enhancement from Cr, Nb, and Mo is strong and that from V, Zr, and Cu is weak, as shown by the linear scanning voltammetry curves in Figure 6E (Qiu et al., 2019a). Jin et al. synthesized a quinary nanoporous AlNiCoIrMo HEA with 2 nm well-aligned nanopores via dealloying. This system exhibits good electrocatalytic activity (overpotential of 233 mV at 10 mA/cm^2) and cycling stability than those Ir-based catalysts in the literature (highest is the result published by Jiang et al. on Ir nanosheets with overpotential of 240 mV at 10 mA/cm^2) (Jiang et al., 2018) that are enhanced by the high-entropy effect and sluggish diffusion effect of HEA (Jin et al., 2019).

It was proposed by Wang et al. that the high-entropy perovskite fluorides of $K(MgMnFeCoNi)F_3$, etc., can act as efficient OER catalysts in alkaline media. The substitution of K with Na can further improve the OER performance. For example, $K_{0.8}Na_{0.2}(MgMnFeCoNi)F_3$ exhibits a low overpotential of 314 mV at a current density of 10 mA/cm^2, which is much lower than that of either IrO_2 or $Ba_{0.5}Sr_{0.5}Co_{0.8}Fe_{0.2}O_{3-d}$ (Wang et al., 2020b). The authors suggest that the superior performance might be benefited from its highly dispersed active sites, low charge transfer resistance, and fast mass transfer enhanced by high entropy.

Oxidation reduction reaction

Pt-based HEA nanostructures have been explored for electrocatalysts for ORR. Li et al. have synthesized nanoporous AlCuNiPtX (X = Pd, V, Co, Mo, etc.) by a selective dealloying method, which provides tunable ORR catalytic performance. Among these quinary alloys, the nanoporous AlCuNiPtMn exhibited high ORR activity and good electrochemical cycling durability, with a half-wave potential of 0.945 V in acidic media which is a $\sim$ 16-fold mass activity of Pt/C. The authors believe that the Mn component enables modulation of the electronic properties and enhances the ORR activity (Li et al., 2020b). Löffler et al. investigated the variation of adsorption energy and ORR activity when adding or replacing components into CrMnFeCoNi NPs (as shown in Figure 7A). Upon adding Nb or Mo, the first two adsorption peaks split and the intrinsic ORR activity improved (Figure 7B). However, adding Cu or replacing Ni by V will reduce the ORR activity. The enhancement of ORR activity might be attributed to the continuous coverage of adsorption energies and the presence of highly active sites at the surface (Figure 7C) (Löffler et al., 2020). The authors also suggested that the high activity not only correlated with synergistic combination of right choice of elements but also was affected by their atomic ratios (Löffler et al., 2018). In another case, Qiu et al. put immiscible elements together into a single-phase nanoporous structure to form senary AlNiCuPtPdAu, octonary AlNiCuPtPdAuCoFe, and senary AlNiCuMoCoFe by a dealloying strategy. The nanoporous AlNiCuPtPdAu exhibited greatly enhanced high-temperature stability (up to 600 °C) and good ORR activity of 10 times mass activity than that of Pt/C (Qiu et al., 2019b). So far, the strategy of Pt-based HEAs for ORR mainly lies in their tunable lattice parameters and electronic structures, which help to optimize the absorption energy. However, more work will be needed to find out the best recipe of elements and more importantly, the rules of optimizing the activity and stability.

CO/CO_2 reduction reaction

Recently, Pedersen et al. proposed an approach combining DFT calculations and supervised machine learning to discover selective and active CORR/CO_2RR catalysts (Figure 8A). This work calculated the CO and H adsorption energies on the (111) surfaces of CoCuGaZnNi and AgAuCuPdPt HEAs. Based on the calculation, they proposed that HEAs with weak hydrogen adsorption could suppress the molecular hydrogen formed, and those with strong CO adsorption on the (111) surfaces could favor the reduction of CO (Pedersen et al., 2020). Nellaiappan et al. found that AuAgPtPdCu exhibited a faradaic efficiency of about 100% toward gaseous products at a low applied potential (−0.3 V versus reversible hydrogen

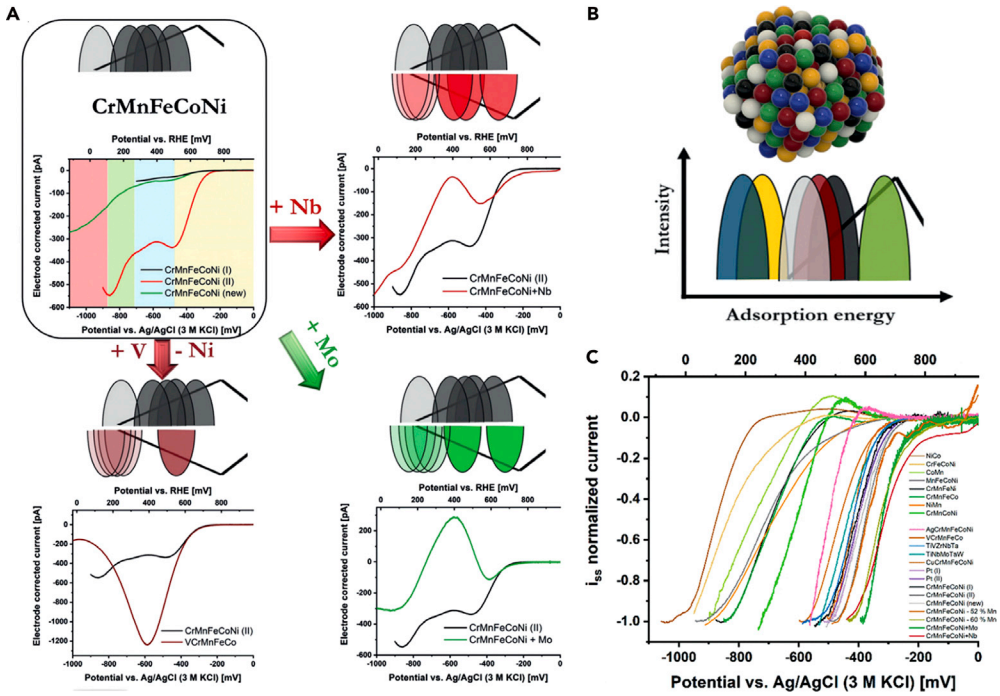

Figure 7. Nanosized HEM electrocatalysts for ORR

(A) Changes of adsorption energy distribution patterns when adding or replacing elements from CrMnFeCoNi.

(B) Schematic illustration of senary HEA nanoparticle with near-continuous adsorption energy distribution.

(C) Comparison of intrinsic activity of different catalysts toward ORR highlighting importance of HEM structure on activity.

Reproduced with permission from Löffler et al. (2020). Copyright © 2020, Wiley-VCH.

electrode), adopting high CO_2RR activity. After comparing with pristine Cu(111) surface, the authors believe that the high activity might be caused by the reversal in adsorption trends for *OCH_3 and *O on Cu(111) and HEA surfaces (Figure 8B). Although many elements are present in this HEA catalysts, the electrocatalytic activity might be predominantly enhanced by the redox-active Cu metal (Cu^{2+}/Cu^0), and other metals provide synergistic effect (Nellaiappan et al., 2020). Chen et al. used a low-temperature mechanochemical method-synthesized (NiMgCuZnCo)O catalysts decorated with noble metal Pt/Ru single atoms or nanoclusters. This mixed HEO shows a good stability at high temperature and a high catalytic activity in the hydrogenation of atmospheric CO_2 to CO (44.9% at 500 °C) (Figure 8C). The HEOs are supposed to be thermodynamically unstable at low temperature; however, the high entropy here lowers Gibbs free energy and helps the homogeneous distribution of cation species and improves the stability (Chen et al., 2019a).

CO oxidation reaction

Chen et al. discovered that $NiMgCuZnCoO_x$ can be used as COOR catalyst, which exhibits a complete CO to CO_2 conversion at 305 °C. To obtain considerable activity for the CO conversion at lower temperature, Pt was introduced into the catalyst to form rock-salt $PtNiMgCuZnCoO_x$. After being reduced in H_2, this catalyst shows a 100% conversion of CO even at 155 °C. The high activity is attributed to the highly dispersed active sites and entropy stabilization (Chen et al., 2018a). On the other hand, the authors prepared a heterostructure of (NiMgCuZnCo)O-$CuCeO_x$ via entropy-driven mechanochemistry. $CuCeO_x$ NPs were decorated on the surface of HEOs, providing catalytic sites for COOR (Chen et al., 2020a). It has also been reported that Cu^{2+} in $Mg_{0.2}Co_{0.2}Ni_{0.2}Cu_{0.2}Zn_{0.2}O$ can be rapidly reduced to Cu^+ by CO at a temperature higher than 130 °C. *Operando* soft X-ray absorption spectroscopy suggests that Cu is the active metal, whereas Co and Ni do not play any role in the COOR. Moreover, Cu^{2+} oxidation state can be easily but slowly recovered by annealing under O_2, which allows the catalytic cycle to continue (Fracchia et al., 2020a). Okejiri et al. used a sonochemical-based method to synthesize monodispersed perovskite HEO NPs with an average crystallite size ~ 5.9 nm. It is shown that Ru/BaSrBi(ZrHfTiFe)O_3 with excellent dispersion of Ru adopts good catalytic activity for COOR. For example, 100% conversion can be achieved at 118°C (Okejiri et al., 2020).

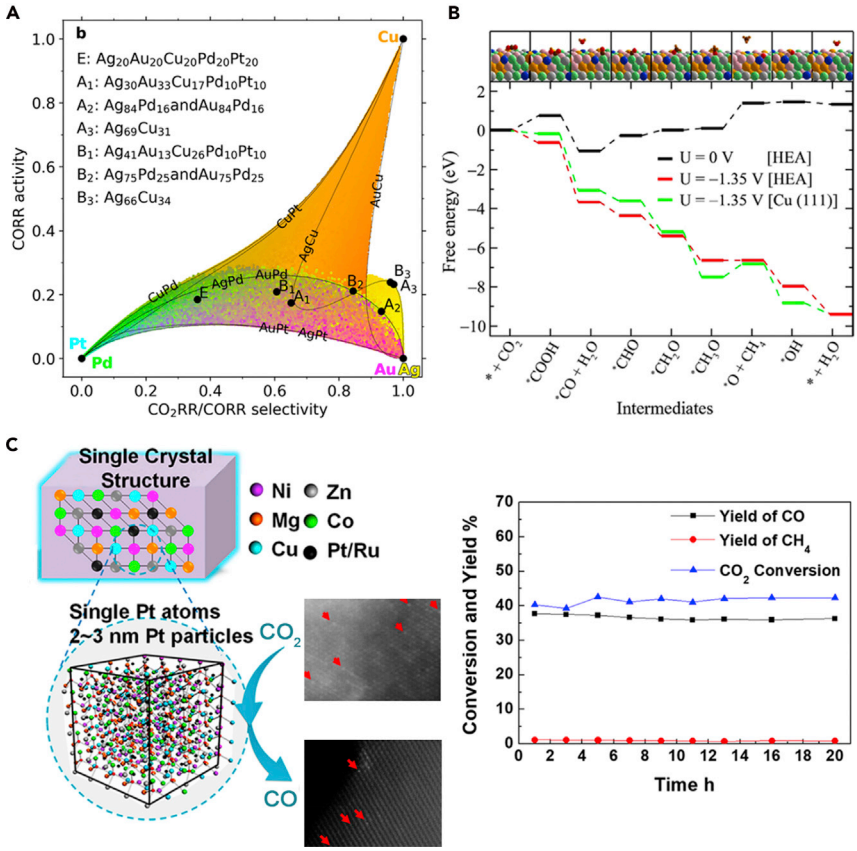

Figure 8. HEM electrocatalysts for CO_2RR/CORR

(A) Plots of the CO_2RR/CORR selectivity and CORR activity space achievable over AgAuCuPdPt NP catalysts. Reproduced with permission from Pedersen et al. (2020). Copyright © 2020, American Chemical Society.

(B) Free-energy diagram of CO_2RR on the AuAgPtPdCu HEA surface. Reproduced with permission from Nellaiappan et al. (2020). Copyright © 2020, American Chemical Society.

(C) Schematic illustration of Pt-(NiMgCuZnCo)O and CO_2 hydrogenation activity. Reproduced with permission from Chen et al. (2019a). Copyright © 2019, American Chemical Society.

Methanol/ethanol oxidation reaction

HEAs composed of Pt-group metals may form not only fcc lattice but also hcp lattice, varying with the component and concentration. Yusenko et al. synthesized hcp structured $Ir_{0.19}Os_{0.22}Re_{0.21}Rh_{0.20}Ru_{0.19}$ and fcc structured $Ir_{0.26}Os_{0.05}Pt_{0.31}Rh_{0.23}Ru_{0.15}$ HEAs via the thermal decomposition of single-source precursor. The former shows a high thermal stability at 1500 K as well as exceptional MOR activity, which was suggested to be due to both electronic and cocktail effects (Yusenko et al., 2017).

Energy storage

Recently, HEOs have been explored for the applications of electrode materials for Li/Na ion batteries, solid electrolytes, and electrode materials for Li-sulfur battery. These applications demand the materials for different properties, such as high capacity, either high electronic conductivity, or high ionic conductivity, etc. The cation tunability of HEOs may fulfill these requests.

Electrode materials in Li ion battery

As shown in Figure 9A, HEOs have been used as both cathode and anode materials for lithium-ion batteries (LIBs) (Oses et al., 2020). Then rational design of HEOs by combining both active and inactive cations is the common strategy for exploring high-performance electrode materials. Most of the investigated HEO electrodes have a rock-salt structure. Lun et al. design high-entropy LIB cathodes with rock-salt structure guided by the DFT calculations. 30% Li excess has been added to ensure good Li transport without severely

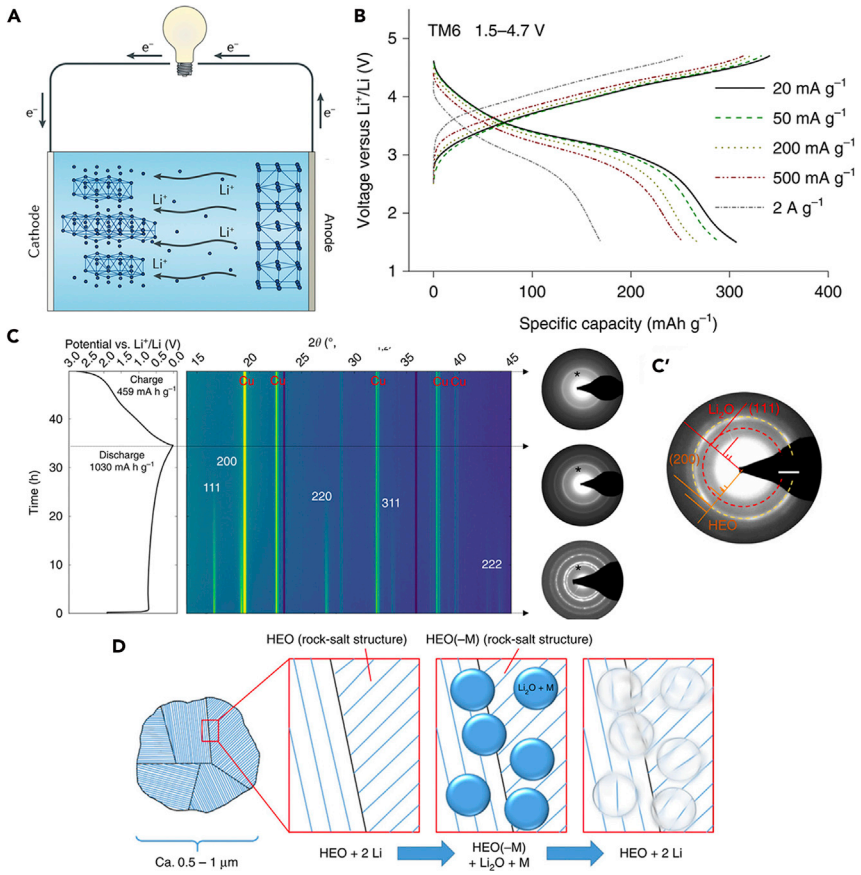

Figure 9. HEM electrodes for lithium storage

(A) Schematic illustration of a rechargeable battery with HEOs as the electrode. Reproduced with permission Oses et al. (2020) and Wang et al. (2019a). Copyright © 2019, Elsevier. Copyright © 2020, Springer Nature.

(B) The first cycle charge-discharge curves of rock-salt TM6 ($Li_{1.3}Mn^{2+}_{0.1}Co^{2+}_{0.1}Mn^{3+}_{0.1}Cr^{3+}_{0.1}Ti_{0.1}Nb_{0.2}O_{1.7}F_{0.3}$) at different currents. Reproduced with permission from Lun et al. (2020). Copyright © 2020, Springer Nature.

(C) *Operando* XRD studies in the first cycle and (C′) SAED pattern from the lithiated sample of $(Co_{0.2}Cu_{0.2}Mg_{0.2}Ni_{0.2}Zn_{0.2})O$ HEO anode.

(D) Schematics of the proposed de-/lithiation mechanism during the conversion reaction of HEO. *M* stands only for the transition metal cations. Reproduced with permission from Sarkar et al. (2018). Copyright © 2018, Springer Nature.

compromising the capacity. By comparing a group of rock-salt cathodes containing two, four, and six transition metal species (TM6: $Li_{1.3}Mn^{2+}_{0.1}Co^{2+}_{0.1}Mn^{3+}_{0.1}Cr^{3+}_{0.1}Ti_{0.1}Nb_{0.2}O_{1.7}F_{0.3}$), they found both energy density and rate capability increased with the number of metal species. TM6 exhibits an excellent rate capability, achieving ~307 mAh/g at a rate of 20 mA/g and ~170 mAh/g at a rate of 2000 mA/g, respectively, as shown in Figure 9B (Lun et al., 2020). Wang et al. synthesized Li-containing HEOF of $Li_x(Co_{0.2}Cu_{0.2}Mg_{0.2}Ni_{0.2}Zn_{0.2})OF_x$ via a facile mechanochemistry method. The HEOF exhibits a potential of 3.4 V versus Li^+/Li, enabling its application as cathode active material due to entropy stabilization (Wang et al., 2019b).

HEO with transition metal cations can serve as anode for LIBs. Sarkar, Chen, Qiu, and Wang et al. studied the rock-salt $(Co_{0.2}Cu_{0.2}Mg_{0.2}Ni_{0.2}Zn_{0.2})O$ for anode of LIBs, respectively (Sarkar et al., 2018; Qiu et al., 2019; Wang et al., 2019a; Chen et al., 2019b). *Operando* XRD and *ex situ* TEM analysis suggest the lithiation reaction of this HEO might be $MO_x + 2xLi \rightarrow M + xLi_2O$, with a capacity of 700–1,000 mAh/g (Figure 9C). The authors suggest that Co^{2+} and Cu^{2+} cations provide capacity with a conversion reaction, whereas the other cations act as matrix to maintain the rock-salt structure. In addition, it is suggested that Mg^{2+} ions are vital in making the HEO structure intact and the rock-salt structure can be preserved after fully lithiation (Figures 9D, [Sarkar et al., 2018]). It has also been proposed by Qiu et al. that a small amount of inactive MgO would

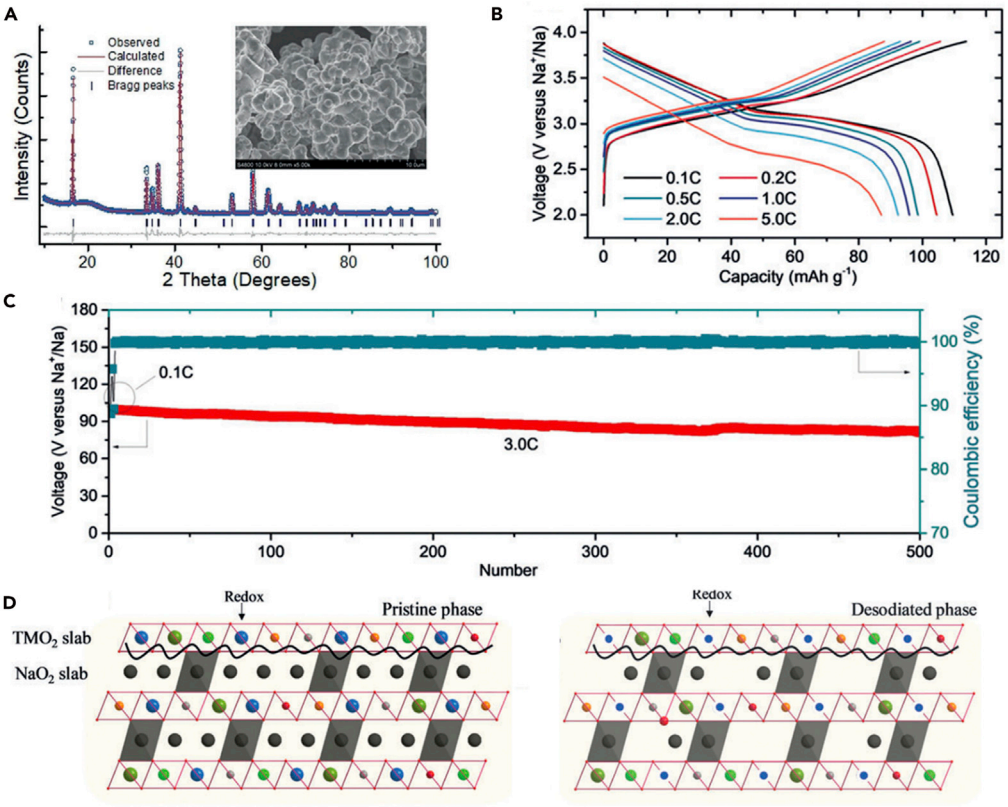

Figure 10. Sodium storage of HEMs

(A) XRD pattern shows the as-prepared $NaNi_{0.12}Cu_{0.12}Mg_{0.12}Fe_{0.15}Co_{0.15}Mn_{0.1}Ti_{0.1}Sn_{0.1}Sb_{0.04}O_2$ HEO with O3-type crystal structure.

(B) Charge-discharge curves cycled at rates from 0.1 to 5.0 C in the voltage range 2.0–3.9 V.

(C) Capacity retention and coulombic efficiency of the O3-type HEO at 3.0 C up to 500 cycles.

(D) Schematic of possible Na^+ (de)intercalation process of the O3-type HEO cathode (left) with multiple transition metals (right). Reproduced with permission from Zhao et al., 2020a. Copyright © 2020, Wiley-VCH.

be formed after the discharge of $(Co_{0.2}Cu_{0.2}Mg_{0.2}Ni_{0.2}Zn_{0.2})O$ HEO, which may help buffer the volume change of the HEO anode and keep the separation of active nanosized crystals (Qiu et al., 2019). Wang et al. has built a full cell with an anode of $(Co_{0.2}Cu_{0.2}Mg_{0.2}Ni_{0.2}Zn_{0.2})O$ and a cathode of $LiNi_{1/3}Co_{1/3}Mn_{1/3}O_2$. The full batteries show pretty good performances, delivering an initial capacity of 446 mAh/g and a capacity of 256 mAh/g after 100 cycles (Wang et al., 2019a).

Lökcü et al. synthesized rock-salt $(MgCoNiZn)_{1-x}Li_xO$ (x = 0.05, 0.15, 0.25, 0.35) anode via a conventional solid-state sintering. XPS analysis revealed that the oxidation of Co and the concentration of oxygen vacancies enhanced by the Li content. The $(MgCoNiZn)_{0.65}Li_{0.35}O$ anode exhibited an initial capacity of 1,930 mAh/g and a discharge capacity of 610 mAh/g after 130 cycles (Lökçü et al., 2020). HEOs with perovskite and spinel structures have also been developed. For example, $(Bi,Na)_{1/5}(La,Li)_{1/5}(Ce,K)_{1/5}Ca_{1/5}Sr_{1/5}]TiO_3$ with perovskite structure shows an initial discharge capacity of 125.9 mAh/g and good stability (Yan et al., 2020). A spinel anode of $(Mg_{0.2}Ti_{0.2}Zn_{0.2}Cu_{0.2}Fe_{0.2})_3O_4$ shows a large reversible capacity of 504 mAh/g at a current density of 100 mA/g after 300 cycles (Chen et al., 2020b).

Electrode materials in Na ion battery

Besides the application in LIBs, it is not surprising to see HEOs being used as electrodes of Na-ion batteries. Zhao et al. have synthesized O3-type $NaNi_{0.12}Cu_{0.12}Mg_{0.12}Fe_{0.15}Co_{0.15}Mn_{0.1}Ti_{0.1}Sn_{0.1}Sb_{0.04}O_2$ via solid-state reaction as cathode (Figure 10A). It is believed that different cations have different roles. For example, cations of N^{i2+}, Cu^{2+}, Fe^{3+}, and Co^{3+} are expected to provide capacity; Mg^{2+} and Ti^{4+} may stabilize the host's structure during cycling; Mn^{2+} can help in the formation of the structure; Sn^{4+} and Sb^{5+} may

raise the average voltage (Sathiya et al., 2018; Yuan et al., 2014). The HEO exhibits a long cycling stability (83% of capacity retention after 500 cycles) as well as a good rate capability, enhanced by the highly reversible O3-P3 phase transition (as shown in Figures 10B and 10C). The authors propose that the multiple transition-metal components may accommodate the changes of local bonds during (de)intercalation, resulting in varied interactions between TMO_2 and NaO_2 slabs, as shown in Figure 10D. During the cycle processes, the size and oxidation states of transition metals that participate in the charge compensation can change. The high entropy composition promotes homogeneous distribution of these redox elements and accommodates the local changes. Consequently, it may help to maintain its layered O3-type structure, supporting the long-term cycling stability as well as better rate performance (Zhao et al., 2020a).

All-solid-state electrolytes

Bérardan et al. synthesized a solid-state HEO electrolyte of $(MgCoNiCu)_{1-x-y}Ga_yA_xO$ (A = Li, Na, K) via solid-state reaction. Impedance spectroscopy measurements reveal that this rock-salt structure has a superionic Li^+ mobility of $\sim 10^{-3}$ S/cm at room temperature as well as a fast ionic Na^+ mobility of 5×10^{-6} S/cm. The authors believe that high ionic conductivity occurring via the oxygen vacancies is created by a charge compensation (Bérardan et al., 2016b). So far, there are not many reports on the application of HEOs on solid electrolyte. To make this kind of electrolyte useful, the chemical stabilities and electrochemical compatibility between electrolyte and electrodes are important for further investigations.

Chemical anchor/sulfur host material/cathode

$(NiMgCuZnCo)O_x$ HEO has also been utilized as the cathode catalyst to anchor the lithium polysulfides (LIPSs) in Li-S batteries. The homogeneously dispersive multiple metal active species in HEO and the synergistic contribution of Li-O and S-Ni bonds favor the restriction of LIPSs and facilitate the redox reaction in the cathode. The authors suggest that this HEO can act as a promoter for polysulfide immobilizing in Li-S batteries with a competitive reversible capacity and a low capacity decay (Zheng et al., 2019).

Hydrogen storage

Shen et al. fabricate an equiatomic HEA of TiZrHfMoNb with the arc-melting method for hydrogen storage. They found this HEA changes its structure from bcc to fcc during hydrogen absorption. The metastable fcc lattice can transform back to bcc during hydrogen desorption at around 302°C. The reversible transformation of this alloy may lead to an improved hydrogen recycling rate and an enhanced energy efficiency for application of solar thermal energy storage (Shen et al., 2019).

Supercapacitor

Kong et al. synthesize nanoporous natured HEAs by dissolving the selective HEA alloys into sulfuric acid solution. Utilized as a binder-free electrode for supercapacitor, nanoporous HEA of AlCoCrFeNi exhibits a high volumetric capacitance of 700 F/cm^3 and an excellent cycling stability of over 3,000 cycles. The good performance may be due to the large surface area from its interconnected large pore channels (Kong et al., 2019). In addition, other HEMs with high surface area were synthesized for the application of supercapacitor. For example, Jin et al. synthesize $(VCrNbMoZr)N_x$ HEN via a mechanochemical-assisted soft urea method. They found that the HEN exhibits a specific capacitance of 78 F/g at a scan rate of 100 mV/s in 1 m KOH solution (Jin et al., 2018). Xu et al. synthesize uniform quinary FeNiCoMnMg ($\sim$ 30 nm) and FeNiCoMnCu ($\sim$ 50 nm) NPs on superaligned electrospun carbon nanofibers via CTS. The latter one exhibits a high capacitance of 203 F/g and a specific energy density of 21.7 Wh/kg (Xu et al., 2020).

Other energy-related applications

Dielectric materials for energy applications

The dielectric compound may store the electric energy via its polarization in the presence of external electric field and therefore be used for various applications such as capacitors, energy harvesting and storage devices, and high-power electronic transducers. Bérardan et al. suggest that (MgCoNiCuZn)O can be substituted by aliovalent ions (+1 or +3) with a charge compensation mechanism, to obtain HEOs as $(MgCoNiCu)_{0.8}(LiGa)_{0.2}O$, $(MgNiCoCuZn)_{0.95}Li_{0.05}O$, and $(MgNiCoCuZn)_{0.84}Li_{0.16}O$. These HEOs exhibit promising colossal dielectric properties in a wide frequency range (2.3 MHz –100 Hz) (Bérardan et al., 2016a). Moreover, high-entropy perovskite $(Na_{0.2}Bi_{0.2}Ba_{0.2}Sr_{0.2}Ca_{0.2})TiO_3$ is reported to produce a discharge energy density of 1.02 J/cm^3 under an electric field of 145 kV/cm, showing promising applications as solid-state refrigeration and energy storage in circuit (Pu et al., 2019).

Magnetic devices

The magnetic properties of functional oxides are dependent on their structure, both atomically and electronically. Meisenheimer et al. take advantage of the inherent chemical and structural disorder of HEO to boost the exchange bias in Permalloy/$(Mg_{0.25(1-x)}Co_xNi_{0.25(1-x)}Cu_{0.25(1-x)}Zn_{0.25(1-x)})O$ heterostructures. The heterostructures are integration of ferromagnetic and antiferromagnetic compounds, which can achieve a 10-fold increase in the exchange interaction depending on the concentration of Co. The authors propose that both local disorder of cations and the concentration of magnetic ions contribute to an improved exchange coupling (Meisenheimer et al., 2017). HEMs containing magnetic ions may serve as a tunable platform for magnetic properties. With proper integration with other functional compounds, HEM-based devices can be explored for applications of magnetic memories, magnetometers, and devices for magneto-optics.

PERSPECTIVES

The past few years have witnessed the emergence of HEMs for energy-related applications, especially catalysis and energy storage. HEMs provide a rich platform for tuning the antisite disordering of atoms within a crystalline structure, for achieving an optimized performance. However, the understanding between the performance and surface structure at atomic level is still not clear. The essential task for developing HEMs is to achieve this structure-property relationship and precisely control their structure and local electronic structure. We briefly list several challenges below. With the help of advanced calculations, syntheses, and characterization tools, these challenges also provide huge opportunities to explore HEMs.

(1) Strategies of designing proper HEMs. Theoretical investigations based on state-of-the-art DFT, molecular dynamics, and others may provide useful guidelines for designing proper HEMs. However, the atomic type disordering may give a huge difficulty in building the atomic model and discovering special constituent combinations for special energy-related applications. Lots of work needs to be done for this goal, and machine learning and other big data approaches may help to deal with the enormous dataset.

(2) Precise structural control of HEMs. Experimentally, synthetic method with controllable manners, simpler operation, and larger scale are still much needed. Strategies of well size, shape, and composition control of HEMs, which are analogous to the case of well-defined metal (including alloy and intermetallic) and semiconductor nanomaterials, remain to be extended.

(3) Advanced characterization. Various advanced techniques, such as X-ray-based technique, SEM, and TEM have been used for structural characterization, which may provide atomically accurate structural and chemical information of HEMs. Developing a technique to address the atomic structure of HEMs quantitatively in 3D would be a challenging task. 3D electron tomography and APT can be promising for this goal.

(4) Thermal stability of HEMs. Although the term "high-entropy" is prevalent in the literature and the idea of using configurational entropy to stabilize a single-phase solid solution is well accepted, the actual contribution of entropy (including configurational, vibrational, electronic, and magnetic entropy) and enthalpy to the total Gibbs free energy are difficult to determine. Attentions are also needed to be paid to the surface strain.

(5) Surface stability at work environment. The surface structure and stability of HEMs during reaction are essential for catalytic applications. This issue is important for catalysis research, but the surface structure of HEMs can be more complicated than the current used catalysts.

(6) Exploration of new types of HEMs. The emergence of HEMs and their energy-related application are still in their infancy. The idea of configuring more than five elements into one lattice may provide infinite combinations. It is also important to investigate how the antisite disordering interplays with other physical parameters, such as strain, 2-dimentional geometry, magnetism, etc. We believe that HEMs will work as important materials platform for future energy and other functional devices.

Resource availability

Lead contact

Further information and requests for resources should be directly to and will be fulfilled by the Lead Contact, Dong Su (dongsu@iphy.ac.cn).

Materials availability

This study did not generate any new unique reagents.

Data and code availability

The data that support the findings of this study are available from the corresponding authors on reasonable request.

METHODS

All methods can be found in the accompanying Transparent Methods supplemental file.

ACKNOWLEDGMENTS

Dong Su acknowledges the support from the Strategic Priority Research Program (B) (grant No. XDB07030200) of Chinese Academy of Sciences. Maosen Fu acknowledges the support of the National Natural Science Foundation of China (Nos. 51972273 and U20A20243), the Innovation and Development Program of Shaanxi Province (No. 2017KTPT-03), the Fundamental Research Funds for the Central Universities (Nos. 3102019JC001, 3102019TS0407), and the Research Fund of the State Key Laboratory of Solidification Processing (NPU), China (No. 2019-TS-14). Xiao Ma acknowledges the support from the Postdoctoral Innovative Talent Support Program and the Natural Science Basic Research Plan in Shaanxi Province of China (No. 2020JQ-167).

AUTHOR CONTRIBUTIONS

Maosen Fu and Xiao Ma wrote the paper and prepared some figures. Kangning Zhao and Xiao Li contributed to the section of Perspectives. Dong Su suggested the proposal and supervised the work. All authors contributed to the revision of manuscript.

DECLARATION OF INTERESTS

The authors declare no competing interests.

REFERENCES

Amiri, A., and Shahbazian-Yassar, R. (2021). Recent progress of high-entropy materials for energy storage and conversion. J. Mater. Chem. A. https://doi.org/10.1039/D0TA09578H.

Batchelor, T.A.A., Pedersen, J.K., Winther, S.H., Castelli, I.E., Jacobsen, K.W., and Rossmeisl, J. (2019). High-entropy alloys as a discovery platform for electrocatalysis. Joule *3*, 834–845, https://doi.org/10.1016/j.joule.2018.12.015.

Bérardan, D., Franger, S., Dragoe, D., Meena, A.K., Dragoe, N., Berardan, D., Franger, S., Dragoe, D., Meena, A.K., and Dragoe, N. (2016a). Colossal dielectric constant in high entropy oxides. Phys. Status Solidi - Rapid Res. Lett. *10*, 328–333, https://doi.org/10.1002/pssr.201600043.

Bérardan, D., Franger, S., Meena, A.K., and Dragoe, N. (2016b). Room temperature lithium superionic conductivity in high entropy oxides. J. Mater. Chem. A. *4*, 9536–9541, https://doi.org/10.1039/c6ta03249d.

Berardan, D., Meena, A.K., Franger, S., Herrero, C., and Dragoe, N. (2017). Controlled Jahn-Teller distortion in (MgCoNiCuZn)O-based high entropy oxides. J. Alloys Compd. *704*, 693–700, https://doi.org/10.1016/j.jallcom.2017.02.070.

Biesuz, M., Fu, S., Dong, J., Jiang, A., Ke, D., Xu, Q., Zhu, D., Bortolotti, M., Reece, M.J., Hu, C., and Grasso, S. (2019). High entropy Sr((Zr0.94Y0.06)0.2Sn0.2Ti0.2Hf0.2Mn0.2)O3−x perovskite synthesis by reactive spark plasma sintering. J. Asian Ceram. Soc. *7*, 127–132, https://doi.org/10.1080/21870764.2019.1595931.

Biesuz, M., Spiridigliozzi, L., Dell'Agli, G., Bortolotti, M., and Sglavo, V.M. (2018). Synthesis and sintering of (Mg, Co, Ni, Cu, Zn)O entropy-stabilized oxides obtained by wet chemical methods. J. Mater. Sci. *53*, 8074–8085, https://doi.org/10.1007/s10853-018-2168-9.

Bondesgaard, M., Broge, N.L.N., Mamakhel, A., Bremholm, M., and Iversen, B.B. (2019). General solvothermal synthesis method for complete solubility range bimetallic and high-entropy alloy nanocatalysts. Adv. Funct. Mater. *29*, 1905933, https://doi.org/10.1002/adfm.201905933.

Broge, N.L.N., Bondesgaard, M., Sondergaard-Pedersen, F., Roelsgaard, M., and Iversen, B.B. (2020). Autocatalytic formation of high-entropy alloy nanoparticles. Angew. Chem. Int. Ed. Engl. *59*, 21920–21924, https://doi.org/10.1002/anie.202009002.

Cantor, B., Chang, I.T.H., Knight, P., and Vincent, A.J.B. (2004). Microstructural development in equiatomic multicomponent alloys. Mater. Sci. Eng. A. *375–377*, 213–218, https://doi.org/10.1016/j.msea.2003.10.257.

Chen, H., Fu, J., Zhang, P., Peng, H., Abney, C.W., Jie, K., Liu, X., Chi, M., and Dai, S. (2018a). Entropy-stabilized metal oxide solid solutions as CO oxidation catalysts with high-temperature stability. J. Mater. Chem. A. *6*, 11129–11133, https://doi.org/10.1039/c8ta01772g.

Chen, H., Jie, K., Jafta, C.J., Yang, Z., Yao, S., Liu, M., Zhang, Z., Liu, J., Chi, M., Fu, J., and Dai, S. (2020a). An ultrastable heterostructured oxide catalyst based on high-entropy materials: a new strategy toward catalyst stabilization via synergistic interfacial interaction. Appl. Catal. B Environ. *276*, 119155, https://doi.org/10.1016/j.apcatb.2020.119155.

Chen, H., Lin, W., Zhang, Z., Jie, K., Mullins, D.R., Sang, X., Yang, S.-Z., Jafta, C.J., Bridges, C.A., Hu, X., et al. (2019a). Mechanochemical synthesis of high entropy oxide materials under ambient conditions: dispersion of catalysts via entropy maximization. ACS Mater. Lett. *1*, 83–88, https://doi.org/10.1021/acsmaterialslett.9b00064.

Chen, H., Qiu, N., Wu, B., Yang, Z., Sun, S., and Wang, Y. (2020b). A new spinel high-entropy oxide (Mg0.2Ti0.2Zn0.2Cu0.2Fe0.2)3O4 with fast reaction kinetics and excellent stability as an anode material for lithium ion batteries. RSC Adv. *10*, 9736–9744, https://doi.org/10.1039/d0ra00255k.

Chen, Hong, Qiu, N., Wu, B., Yang, Z., Sun, S., and Wang, Y. (2019b). Tunable pseudocapacitive contribution by dimension control in nanocrystalline-constructed (Mg 0.2 Co 0.2 Ni 0.2 Cu 0.2 Zn 0.2)O solid solutions to achieve superior lithium-storage properties. RSC Adv. *9*,

28908–28915, https://doi.org/10.1039/C9RA05508H.

Chen, K., Pei, X., Tang, L., Cheng, H., Li, Z., Li, C., Zhang, X., and An, L. (2018b). A five-component entropy-stabilized fluorite oxide. J. Eur. Ceram. Soc. *38*, 4161–4164, https://doi.org/10.1016/j.jeurceramsoc.2018.04.063.

Chen, X., Si, C., Gao, Y., Frenzel, J., Sun, J., Eggeler, G., and Zhang, Z. (2015). Multi-component nanoporous platinum–ruthenium–copper–osmium–iridium alloy with enhanced electrocatalytic activity towards methanol oxidation and oxygen reduction. J. Power Sourc. *273*, 324–332, https://doi.org/10.1016/j.jpowsour.2014.09.076.

Dąbrowa, J., Olszewska, A., Falkenstein, A., Schwab, C., Szymczak, M., Zajusz, M., Moździerz, M., Mikuła, A., Zielińska, K., Berent, K., et al. (2020). An innovative approach to design SOFC air electrode materials: high entropy La 1−x Sr x (Co,Cr,Fe,Mn,Ni)O 3−δ (x = 0, 0.1, 0.2, 0.3) perovskites synthesized by the sol–gel method. J. Mater. Chem. A. *8*, 24455–24468, https://doi.org/10.1039/D0TA06356H.

Dąbrowa, J., Stygar, M., Mikuła, A., Knapik, A., Mroczka, K., Tejchman, W., Danielewski, M., and Martin, M. (2018). Synthesis and microstructure of the (Co,Cr,Fe,Mn,Ni)3O4 high entropy oxide characterized by spinel structure. Mater. Lett. *216*, 32–36, https://doi.org/10.1016/j.matlet.2017.12.148.

Dai, S. (2020). Across the board: sheng Dai on catalyst design by entropic factors. ChemSusChem *13*, 1915–1917, https://doi.org/10.1002/cssc.202000448.

Dai, W., Lu, T., and Pan, Y. (2019). Novel and promising electrocatalyst for oxygen evolution reaction based on MnFeCoNi high entropy alloy. J. Power Sourc. *430*, 104–111, https://doi.org/10.1016/j.jpowsour.2019.05.030.

Ding, Q., Zhang, Y., Chen, X., Fu, X., Chen, D., Chen, S., Gu, L., Wei, F., Bei, H., Gao, Y., et al. (2019). Tuning element distribution, structure and properties by composition in high-entropy alloys. Nature *574*, 223–227, https://doi.org/10.1038/s41586-019-1617-1.

Djenadic, R., Sarkar, A., Clemens, O., Loho, C., Botros, M., Chakravadhanula, V.S.K., Kübel, C., Bhattacharya, S.S., Gandhi, A.S., and Hahn, H. (2017). Multicomponent equiatomic rare earth oxides. Mater. Res. Lett. *5*, 102–109, https://doi.org/10.1080/21663831.2016.1220433.

Dragoe, N., and Bérardan, D. (2019). Order emerging from disorder. Science *366*, 573–574, https://doi.org/10.1126/science.aaz1598.

Feng, D., Dong, Y., Zhang, L., Ge, X., Zhang, W., Dai, S., and Qiao, Z.-A. (2020a). Holey lamellar high-entropy oxide as an ultra-high-activity heterogeneous catalyst for solvent-free aerobic oxidation of benzyl alcohol. Angew. Chem. Int. Ed. *59*, 2–9, https://doi.org/10.1002/anie.202004892.

Feng, J., Chen, D., Pikhitsa, P.V., Jung, Y., Yang, J., and Choi, M. (2020b). Unconventional alloys confined in nanoparticles: building blocks for new matter. Matter *3*, 1646–1663, https://doi.org/10.1016/j.matt.2020.07.027.

Fracchia, M., Ghigna, P., Pozzi, T., Anselmi Tamburini, U., Colombo, V., Braglia, L., and Torelli, P. (2020a). Stabilization by configurational entropy of the Cu(II) active site during CO oxidation on Mg 0.2 Co 0.2 Ni 0.2 Cu 0.2 Zn 0.2 O. J. Phys. Chem. Lett. *11*, 3589–3593, https://doi.org/10.1021/acs.jpclett.0c00602.

Fracchia, M., Manzoli, M., Anselmi-Tamburini, U., and Ghigna, P. (2020b). A new eight-cation inverse high entropy spinel with large configurational entropy in both tetrahedral and octahedral sites: synthesis and cation distribution by X-ray absorption spectroscopy. Scr. Mater. *188*, 26–31, https://doi.org/10.1016/j.scriptamat.2020.07.002.

Gao, S., Hao, S., Huang, Z., Yuan, Y., Han, S., Lei, L., Zhang, X., Shahbazian-Yassar, R., and Lu, J. (2020). Synthesis of high-entropy alloy nanoparticles on supports by the fast moving bed pyrolysis. Nat. Commun. *11*, 2016, https://doi.org/10.1038/s41467-020-15934-1.

George, E.P., Raabe, D., and Ritchie, R.O. (2019). High-entropy alloys. Nat. Rev. Mater. *4*, 515–534, https://doi.org/10.1038/s41578-019-0121-4.

Gild, J., Kaufmann, K., Vecchio, K., and Luo, J. (2019). Reactive flash spark plasma sintering of high-entropy ultrahigh temperature ceramics. Scr. Mater. *170*, 106–110, https://doi.org/10.1016/j.scriptamat.2019.05.039.

Gild, J., Zhang, Y., Harrington, T., Jiang, S., Hu, T., Quinn, M.C., Mellor, W.M., Zhou, N., Vecchio, K., and Luo, J. (2016). High-entropy metal diborides: a new class of high-entropy materials and a new type of ultrahigh temperature ceramics. Sci. Rep. *6*, 2–11, https://doi.org/10.1038/srep37946.

Glasscott, M.W., Pendergast, A.D., Goines, S., Bishop, A.R., Hoang, A.T., Renault, C., and Dick, J.E. (2019). Electrosynthesis of high-entropy metallic glass nanoparticles for designer, multi-functional electrocatalysis. Nat. Commun. *10*, 2650, https://doi.org/10.1038/s41467-019-10303-z.

Gludovatz, B., Hohenwarter, A., Catoor, D., Chang, E.H., George, E.P., and Ritchie, R.O. (2014). A fracture-resistant high-entropy alloy for cryogenic applications. Science *345*, 1153–1158, https://doi.org/10.1126/science.1254581.

Gorsse, S., Miracle, D.B., and Senkov, O.N. (2017). Mapping the world of complex concentrated alloys. Acta Mater. *135*, 177–187, https://doi.org/10.1016/j.actamat.2017.06.027.

Hu, J., Shen, H., Jiang, M., Gong, H., Xiao, H., Liu, Z., Sun, G., and Zu, X. (2019). A DFT study of hydrogen storage in high-entropy alloy TiZrHfScMo. Nanomater *9*, 461, https://doi.org/10.3390/nano9030461.

Huang, K., Zhang, B., Wu, J., Zhang, T., Peng, D., Cao, X., Zhang, Z., Li, Z., and Huang, Y. (2020). Exploring the impact of atomic lattice deformation on oxygen evolution reactions based on a sub-5 nm pure face-centred cubic high-entropy alloy electrocatalyst. J. Mater. Chem. A. *8*, 11938–11947, https://doi.org/10.1039/d0ta02125c.

Jiang, B., Guo, Y., Kim, J., Whitten, A.E., Wood, K., Kani, K., Rowan, A.E., Henzie, J., and Yamauchi, Y. (2018). Mesoporous metallic iridium nanosheets. J. Am. Chem. Soc. *140*, 12434–12441, https://doi.org/10.1021/jacs.8b05206.

Jimenez-Segura, M.P., Takayama, T., Bérardan, D., Hoser, A., Reehuis, M., Takagi, H., and Dragoe, N. (2019). Long-range magnetic ordering in rocksalt-type high-entropy oxides. Appl. Phys. Lett. *114*, 122401, https://doi.org/10.1063/1.5091787.

Jin, T., Sang, X., Unocic, R.R., Kinch, R.T., Liu, X., Hu, J., Liu, H., and Dai, S. (2018). Mechanochemical-assisted synthesis of high-entropy metal nitride via a soft urea strategy. Adv. Mater. *30*, 1707512, https://doi.org/10.1002/adma.201707512.

Jin, Z., Lv, J., Jia, H., Liu, W., Li, H., Chen, Z., Lin, X., Xie, G., Liu, X., Sun, S., and Qiu, H. (2019). Nanoporous Al-Ni-Co-Ir-Mo high-entropy alloy for record-high water splitting activity in acidic environments. Small *15*, 1904180, https://doi.org/10.1002/smll.201904180.

Katiyar, N.K., Nellaiappan, S., Kumar, R., Malviya, K.D., Pradeep, K.G., Singh, A.K., Sharma, S., Tiwary, C.S., and Biswas, K. (2020). Formic acid and methanol electro-oxidation and counter hydrogen production using nano high entropy catalyst. Mater. Today Energy *16*, https://doi.org/10.1016/j.mtener.2020.100393.

Kong, K., Hyun, J., Kim, Y., Kim, W., and Kim, D. (2019). Nanoporous structure synthesized by selective phase dissolution of AlCoCrFeNi high entropy alloy and its electrochemical properties as supercapacitor electrode. J. Power Sourc. *437*, 226927, https://doi.org/10.1016/j.jpowsour.2019.226927.

Kotsonis, G.N., Rost, C.M., Harris, D.T., and Maria, J.P. (2018). Epitaxial entropy-stabilized oxides: growth of chemically diverse phases via kinetic bombardment. MRS Commun. *8*, 1371–1377, https://doi.org/10.1557/mrc.2018.184.

Lacey, S.D., Dong, Q., Huang, Z., Luo, J., Xie, H., Lin, Z., Kirsch, D.J., Vattipalli, V., Povinelli, C., Fan, W., et al. (2019). Stable multimetallic nanoparticles for oxygen electrocatalysis. Nano Lett. *19*, 5149–5158, https://doi.org/10.1021/acs.nanolett.9b01523.

Lei, Z., Liu, X., Wu, Y., Wang, H., Jiang, S., Wang, S., Hui, X., Wu, Y., Gault, B., Kontis, P., et al. (2018). Enhanced strength and ductility in a high-entropy alloy via ordered oxygen complexes. Nature *563*, 546–550, https://doi.org/10.1038/s41586-018-0685-y.

Li, H., Han, Y., Zhao, H., Qi, W., Zhang, D., Yu, Y., Cai, W., Li, S., Lai, J., Huang, B., and Wang, L. (2020a). Fast site-to-site electron transfer of high-entropy alloy nanocatalyst driving redox electrocatalysis. Nat. Commun. *11*, 5437, https://doi.org/10.1038/s41467-020-19277-9.

Li, S., Tang, X., Jia, H., Li, H., Xie, G., Liu, X., Lin, X., and Qiu, H.J. (2020b). Nanoporous high-entropy alloys with low Pt loadings for high-performance electrochemical oxygen reduction. J. Catal. *383*, 164–171, https://doi.org/10.1016/j.jcat.2020.01.024.

Li, Z., Pradeep, K.G., Deng, Y., Raabe, D., and Tasan, C.C. (2016). Metastable high-entropy dual-phase alloys overcome the strength–ductility trade-off. Nature *534*, 227–230, https://doi.org/10.1038/nature17981.

Li, Z., Zhao, S., Ritchie, R.O., and Meyers, M.A. (2019). Mechanical properties of high-entropy alloys with emphasis on face-centered cubic alloys. Prog. Mater. Sci. *102*, 296–345, https://doi.org/10.1016/j.pmatsci.2018.12.003.

Liu, D., Peng, X., Liu, J., Chen, L., Yang, Y., and An, L. (2020). Ultrafast synthesis of entropy-stabilized oxide at room temperature. J. Eur. Ceram. Soc. *40*, 2504–2508, https://doi.org/10.1016/j.jeurceramsoc.2020.01.018.

Liu, D., Wen, T., Ye, B., and Chu, Y. (2019a). Synthesis of superfine high-entropy metal diboride powders. Scr. Mater. *167*, 110–114, https://doi.org/10.1016/j.scriptamat.2019.03.038.

Liu, M., Zhang, Z., Okejiri, F., Yang, S., Zhou, S., and Dai, S. (2019b). Entropy-maximized synthesis of multimetallic nanoparticle catalysts via a ultrasonication-assisted wet chemistry method under ambient conditions. Adv. Mater. Inter. *6*, 1–6, https://doi.org/10.1002/admi.201900015.

Löffler, T., Meyer, H., Savan, A., Wilde, P., Garzón Manjón, A., Chen, Y.-T., Ventosa, E., Scheu, C., Ludwig, A., and Schuhmann, W. (2018). Discovery of a multinary noble metal-free oxygen reduction catalyst. Adv. Energy Mater. *8*, 1802269, https://doi.org/10.1002/aenm.201802269.

Löffler, T., Savan, A., Garzón-Manjón, A., Meischein, M., Scheu, C., Ludwig, A., and Schuhmann, W. (2019). Toward a paradigm shift in electrocatalysis using complex solid solution nanoparticles. ACS Energy Lett. *4*, 1206–1214, https://doi.org/10.1021/acsenergylett.9b00531.

Löffler, T., Savan, A., Meyer, H., Meischein, M., Strotkötter, V., Ludwig, A., and Schuhmann, W. (2020). Design of complex solid-solution electrocatalysts by correlating configuration, adsorption energy distribution patterns, and activity curves. Angew. Chem. Int. Ed. *59*, 5844–5850, https://doi.org/10.1002/anie.201914666.

Lökçü, E., Toparli, Ç., and Anik, M. (2020). Electrochemical performance of (MgCoNiZn) 1– x Li x O high-entropy oxides in lithium-ion batteries. ACS Appl. Mater. Inter. *7*, 0c03562, https://doi.org/10.1021/acsami.0c03562.

Lun, Z., Ouyang, B., Kwon, D.-H., Ha, Y., Foley, E.E., Huang, T.-Y., Cai, Z., Kim, H., Balasubramanian, M., Sun, Y., et al. (2020). Cation-disordered rocksalt-type high-entropy cathodes for Li-ion batteries. Nat. Mater. https://doi.org/10.1038/s41563-020-00816-0.

Lv, Z.Y., Liu, X.J., Jia, B., Wang, H., Wu, Y., and Lu, Z.P. (2016). Development of a novel high-entropy alloy with eminent efficiency of degrading azo dye solutions. Sci. Rep. *6*, 1–11, https://doi.org/10.1038/srep34213.

Mao, A., Xiang, H.Z., Zhang, Z.G., Kuramoto, K., Zhang, H., and Jia, Y. (2020). A new class of spinel high-entropy oxides with controllable magnetic properties. J. Magn. Magn. Mater. *497*, 1–5, https://doi.org/10.1016/j.jmmm.2019.165884.

Meisenheimer, P.B., Kratofil, T.J., and Heron, J.T. (2017). Giant enhancement of exchange coupling in entropy-stabilized oxide heterostructures. Sci. Rep. *7*, 13344, https://doi.org/10.1038/s41598-017-13810-5.

Miracle, D.B., and Senkov, O.N. (2017a). A critical review of high entropy alloys and related concepts. ACTA Mater. *122*, 448–511, https://doi.org/10.1016/j.actamat.2016.08.081.

Miracle, D.B., and Senkov, O.N. (2017b). A critical review of high entropy alloys and related concepts. Acta Mater. https://doi.org/10.1016/j.actamat.2016.08.081.

Nellaiappan, S., Katiyar, N.K., Kumar, R., Parui, A., Malviya, K.D., Pradeep, K.G., Singh, A.K., Sharma, S., Tiwary, C.S., and Biswas, K. (2020). High-entropy alloys as catalysts for the CO 2 and CO reduction reactions: experimental realization. ACS Catal. *10*, 3658–3663, https://doi.org/10.1021/acscatal.9b04302.

Nguyen, T.X., Patra, J., Chang, J.-K., and Ting, J.-M. (2020). High entropy spinel oxide nanoparticles for superior lithiation–delithiation performance. J. Mater. Chem. A. *8*, 18963–18973, https://doi.org/10.1039/D0TA04844E.

Niu, B., Zhang, F., Ping, H., Li, N., Zhou, J., Lei, L., Xie, J., Zhang, J., Wang, W., and Fu, Z. (2017). Sol-gel autocombustion synthesis of nanocrystalline high-entropy alloys. Sci. Rep. *7*, 3421, https://doi.org/10.1038/s41598-017-03644-6.

Okejiri, F., Zhang, Z., Liu, J., Liu, M., Yang, S., and Dai, S. (2020). Room-temperature synthesis of high-entropy perovskite oxide nanoparticle catalysts through ultrasonication-based method. ChemSusChem *13*, 111–115, https://doi.org/10.1002/cssc.201902705.

Oses, C., Toher, C., and Curtarolo, S. (2020). High-entropy ceramics. Nat. Rev. Mater. *5*, 295–309, https://doi.org/10.1038/s41578-019-0170-8.

Ostovari Moghaddam, A., and Trofimov, E.A. (2021). Toward expanding the realm of high entropy materials to platinum group metals: a review. J. Alloys Compd. *851*, 156838, https://doi.org/10.1016/j.jallcom.2020.156838.

Parida, T., Karati, A., Guruvidyathri, K., Murty, B.S., and Markandeyulu, G. (2020). Novel rare-earth and transition metal-based entropy stabilized oxides with spinel structure. Scr. Mater. *178*, 513–517, https://doi.org/10.1016/j.scriptamat.2019.12.027.

Park, J.H., and Ahn, H.S. (2020). Electrochemical synthesis of multimetallic nanoparticles and their application in alkaline oxygen reduction catalysis. Appl. Surf. Sci. *504*, https://doi.org/10.1016/j.apsusc.2019.144517.

Patel, R.K., Ojha, S.K., Kumar, S., Saha, A., Mandal, P., Freeland, J.W., and Middey, S. (2020). Epitaxial stabilization of ultra thin films of high entropy perovskite. Appl. Phys. Lett. *116*, 071601, https://doi.org/10.1063/1.5133710.

Pedersen, J.K., Batchelor, T.A.A., Bagger, A., and Rossmeisl, J. (2020). High-entropy alloys as catalysts for the CO 2 and CO reduction reactions. ACS Catal. *10*, 2169–2176, https://doi.org/10.1021/acscatal.9b04343.

Pu, Y., Zhang, Q., Li, R., Chen, M., Du, X., and Zhou, S. (2019). Dielectric properties and electrocaloric effect of high-entropy (Na0.2Bi0.2Ba0.2Sr0.2Ca0.2)TiO3 ceramic. Appl. Phys. Lett. *115*, 0–5, https://doi.org/10.1063/1.5126652.

Qiu, H.-J., Fang, G., Gao, J., Wen, Y., Lv, J., Li, H., Xie, G., Liu, X., and Sun, S. (2019a). Noble metal-free nanoporous high-entropy alloys as highly efficient electrocatalysts for oxygen evolution reaction. ACS Mater. Lett. *1*, 526–533, https://doi.org/10.1021/acsmaterialslett.9b00414.

Qiu, H.-J., Fang, G., Wen, Y., Liu, P., Xie, G., Liu, X., and Sun, S. (2019b). Nanoporous high-entropy alloys for highly stable and efficient catalysts. J. Mater. Chem. A. *7*, 6499–6506, https://doi.org/10.1039/C9TA00505F.

Qiu, N., Chen, H., Yang, Z., Sun, S., Wang, Y., and Cui, Y. (2019). A high entropy oxide (Mg0.2Co0.2Ni0.2Cu0.2Zn0.2O) with superior lithium storage performance. J. Alloys Compd. *777*, 767–774, https://doi.org/10.1016/j.jallcom.2018.11.049.

Rák, Z., Maria, J.-P., and Brenner, D.W. (2018). Evidence for Jahn-Teller compression in the (Mg, Co, Ni, Cu, Zn)O entropy-stabilized oxide: a DFT study. Mater. Lett. *217*, 300–303, https://doi.org/10.1016/j.matlet.2018.01.111.

Rost, C.M., Rak, Z., Brenner, D.W., and Maria, J.-P. (2017). Local structure of the Mg x Ni x Co x Cu x Zn x O(x =0.2) entropy-stabilized oxide: an EXAFS study. J. Am. Ceram. Soc. *100*, 2732–2738, https://doi.org/10.1111/jace.14756.

Rost, C.M., Sachet, E., Borman, T., Moballegh, A., Dickey, E.C., Hou, D., Jones, J.L., Curtarolo, S., and Maria, J.-P. (2015). Entropy-stabilized oxides. Nat. Commun. *6*, 8485, https://doi.org/10.1038/ncomms9485.

Sarkar, A., Breitung, B., and Hahn, H. (2020a). High entropy oxides: the role of entropy, enthalpy and synergy. Scr. Mater. *187*, 43–48, https://doi.org/10.1016/j.scriptamat.2020.05.019.

Sarkar, A., Djenadic, R., Usharani, N.J., Sanghvi, K.P., Chakravadhanula, V.S.K., Gandhi, A.S., Hahn, H., and Bhattacharya, S.S. (2017). Nanocrystalline multicomponent entropy stabilised transition metal oxides. J. Eur. Ceram. Soc. *37*, 747–754, https://doi.org/10.1016/j.jeurceramsoc.2016.09.018.

Sarkar, A., Eggert, B., Velasco, L., Mu, X., Lill, J., Ollefs, K., Bhattacharya, S.S., Wende, H., Kruk, R., Brand, R.A., and Hahn, H. (2020b). Role of intermediate 4 f states in tuning the band structure of high entropy oxides. APL Mater. *8*, 051111, https://doi.org/10.1063/5.0007944.

Sarkar, A., Velasco, L., Wang, D., Wang, Q., Talasila, G., de Biasi, L., Kübel, C., Brezesinski, T., Bhattacharya, S.S., Hahn, H., and Breitung, B. (2018). High entropy oxides for reversible energy storage. Nat. Commun. *9*, 3400, https://doi.org/10.1038/s41467-018-05774-5.

Sarker, P., Harrington, T., Toher, C., Oses, C., Samiee, M., Maria, J.-P., Brenner, D.W., Vecchio, K.S., and Curtarolo, S. (2018). High-entropy high-hardness metal carbides discovered by entropy descriptors. Nat. Commun. *9*, 4980, https://doi.org/10.1038/s41467-018-07160-7.

Sathiya, M., Jacquet, Q., Doublet, M.-L., Karakulina, O.M., Hadermann, J., and Tarascon, J.-M. (2018). A chemical approach to raise cell voltage and suppress phase transition in O3 sodium layered oxide electrodes. Adv. Energy

Mater. *8*, https://doi.org/10.1002/aenm.201702599.

Shen, H., Zhang, Jianwei, Hu, J., Zhang, Jinchao, Mao, Y., Xiao, H., Zhou, X., and Zu, X. (2019). A novel TiZrHfMoNb high-entropy alloy for solar thermal energy storage. Nanomaterials *9*, 1–9, https://doi.org/10.3390/nano9020248.

Stygar, M., Dąbrowa, J., Moździerz, M., Zajusz, M., Skubida, W., Mroczka, K., Berent, K., Świerczek, K., and Danielewski, M. (2020). Formation and properties of high entropy oxides in Co-Cr-Fe-Mg-Mn-Ni-O system: novel (Cr,Fe,Mg,Mn,Ni)3O4 and (Co,Cr,Fe,Mg,Mn)3O4 high entropy spinels. J. Eur. Ceram. Soc. *40*, 1644–1650, https://doi.org/10.1016/j.jeurceramsoc.2019.11.030.

Sure, J., Sri Maha Vishnu, D., Kim, H.-K., and Schwandt, C. (2020). Facile electrochemical synthesis of nanoscale (TiNbTaZrHf)C high-entropy carbide. Powder. Angew. Chem. Int. Ed. *59*, 11830–11835, https://doi.org/10.1002/anie.202003530.

Tomboc, G.M., Kwon, T., Joo, J., and Lee, K. (2020). High entropy alloy electrocatalysts: a critical assessment of fabrication and performance. J. Mater. Chem. A. *8*, 14844–14862, https://doi.org/10.1039/D0TA05176D.

Tsai, C.-F., Yeh, K.-Y., Wu, P.-W., Hsieh, Y.-F., and Lin, P. (2009). Effect of platinum present in multi-element nanoparticles on methanol oxidation. J. Alloys Compd. *478*, 868–871, https://doi.org/10.1016/j.jallcom.2008.12.055.

Usharani, N.J., Bhandarkar, A., Subramanian, S., and Bhattacharya, S.S. (2020). Antiferromagnetism in a nanocrystalline high entropy oxide (Co,Cu,Mg,Ni,Zn)O: magnetic constituents and surface anisotropy leading to lattice distortion. Acta Mater. *200*, 526–536, https://doi.org/10.1016/j.actamat.2020.09.034.

Waag, F., Li, Y., Ziefuß, A.R., Bertin, E., Kamp, M., Duppel, V., Marzun, G., Kienle, L., Barcikowski, S., and Gökce, B. (2019). Kinetically-controlled laser-synthesis of colloidal high-entropy alloy nanoparticles. RSC Adv. *9*, 18547–18558, https://doi.org/10.1039/c9ra03254a.

Wang, A.L., Wan, H.C., Xu, H., Tong, Y.X., and Li, G.R. (2014). Quinary PdNiCoCuFe alloy nanotube Arrays as efficient electrocatalysts for methanol oxidation. Electrochim. Acta *127*, 448–453, https://doi.org/10.1016/j.electacta.2014.02.076.

Wang, D., Liu, Z., Du, S., Zhang, Y., Li, H., Xiao, Z., Chen, W., Chen, R., Wang, Y., Zou, Y., and Wang, S. (2019). Low-temperature synthesis of small-sized high-entropy oxides for water oxidation. J. Mater. Chem. A. *7*, 24211–24216, https://doi.org/10.1039/c9ta08740k.

Wang, K., Ma, B., Li, T., Xie, C., Sun, Z., Liu, D., Liu, J., and An, L. (2020a). Fabrication of high-entropy perovskite oxide by reactive flash sintering. Ceram. Int. *46*, 18358–18361, https://doi.org/10.1016/j.ceramint.2020.04.060.

Wang, Q., Sarkar, A., Li, Z., Lu, Y., Velasco, L., Bhattacharya, S.S., Brezesinski, T., Hahn, H., and Breitung, B. (2019a). High entropy oxides as anode material for Li-ion battery applications: a practical approach. Electrochem. Commun. *100*, 121–125, https://doi.org/10.1016/j.elecom.2019.02.001.

Wang, Q., Sarkar, A., Wang, D., Velasco, L., Azmi, R., Bhattacharya, S.S., Bergfeldt, T., Düvel, A., Heitjans, P., Brezesinski, T., et al. (2019b). Multi-anionic and -cationic compounds: new high entropy materials for advanced Li-ion batteries. Energy Environ. Sci. *12*, 2433–2442, https://doi.org/10.1039/C9EE00368A.

Wang, S., and Xin, H. (2019). Predicting catalytic activity of high-entropy alloys for electrocatalysis. Chem *5*, 502–504, https://doi.org/10.1016/j.chempr.2019.02.015.

Wang, T., Chen, H., Yang, Z., Liang, J., and Dai, S. (2020b). High-entropy perovskite fluorides: a new platform for oxygen evolution catalysis. J. Am. Chem. Soc. *142*, 4550–4554, https://doi.org/10.1021/jacs.9b12377.

Wu, D., Kusada, K., Yamamoto, T., Toriyama, T., Matsumura, S., Gueye, I., Seo, O., Kim, J., Hiroi, S., Sakata, O., et al. (2020a). On the electronic structure and hydrogen evolution reaction activity of platinum group metal-based high-entropy-alloy nanoparticles. Chem. Sci. https://doi.org/10.1039/D0SC02351E.

Wu, D., Kusada, K., Yamamoto, T., Toriyama, T., Matsumura, S., Kawaguchi, S., Kubota, Y., and Kitagawa, H. (2020b). Platinum-group-metal high-entropy-alloy nanoparticles. J. Am. Chem. Soc. *142*, 13833–13838, https://doi.org/10.1021/jacs.0c04807.

Xiang, H.-Z., Xie, H.-X., Mao, A., Jia, Y.-G., and Si, T.-Z. (2020). Facile preparation of single phase high-entropy oxide nanocrystalline powders by solution combustion synthesis. Int. J. Mater. Res. *111*, 246–249, https://doi.org/10.3139/146.111874.

Xie, P., Yao, Y., Huang, Z., Liu, Z., Zhang, J., Li, T., Wang, G., Shahbazian-Yassar, R., Hu, L., and Wang, C. (2019). Highly efficient decomposition of ammonia using high-entropy alloy catalysts. Nat. Commun. *10*, 1–12, https://doi.org/10.1038/s41467-019-11848-9.

Xin, Y., Li, S., Qian, Y., Zhu, W., Yuan, H., Jiang, P., Guo, R., and Wang, L. (2020). High-entropy alloys as a platform for catalysis: progress, challenges, and opportunities. ACS Catal. 11280–11306, https://doi.org/10.1021/acscatal.0c03617.

Xu, X., Du, Y., Wang, C., Guo, Y., Zou, J., Zhou, K., Zeng, Z., Liu, Y., and Li, L. (2020). High-entropy alloy nanoparticles on aligned electronspun carbon nanofibers for supercapacitors. J. Alloys Compd. *822*, 153642, https://doi.org/10.1016/j.jallcom.2020.153642.

Yalamanchili, K., Wang, F., Schramm, I.C., Andersson, J.M., Johansson Jöesaar, M.P., Tasnádi, F., Mücklich, F., Ghafoor, N., and Odén, M. (2017). Exploring the high entropy alloy concept in (AlTiVNbCr)N. Thin Solid Films *636*, 346–352, https://doi.org/10.1016/j.tsf.2017.06.029.

Yan, J., Wang, D., Zhang, X., Li, J., Du, Q., Liu, X., Zhang, J., and Qi, X. (2020). A high-entropy perovskite titanate lithium-ion battery anode. J. Mater. Sci. *55*, 6942–6951, https://doi.org/10.1007/s10853-020-04482-0.

Yan, X., and Zhang, Y. (2020). Functional properties and promising applications of high entropy alloys. Scr. Mater. *187*, 188–193, https://doi.org/10.1016/j.scriptamat.2020.06.017.

Yang, Y., Song, B., Ke, X., Xu, F., Bozhilov, K.N., Hu, L., Shahbazian-Yassar, R., and Zachariah, M.R. (2020). Aerosol synthesis of high entropy alloy nanoparticles. Langmuir *36*, 1985–1992, https://doi.org/10.1021/acs.langmuir.9b03392.

Yao, Y., Huang, Z., Li, T., Wang, H., Liu, Y., Stein, H.S., Mao, Y., Gao, J., Jiao, M., Dong, Q., et al. (2020a). High-throughput, combinatorial synthesis of multimetallic nanoclusters. Proc. Natl. Acad. Sci. U S A. *117*, 6316–6322, https://doi.org/10.1073/pnas.1903721117.

Yao, Y., Huang, Z., Xie, P., Lacey, S.D., Jacob, R.J., Xie, H., Chen, F., Nie, A., Pu, T., Rehwoldt, M., et al. (2018). Carbothermal shock synthesis of high-entropy-alloy nanoparticles. Science *359*, 1489–1494, https://doi.org/10.1126/science.aan5412.

Yao, Y., Liu, Z., Xie, P., Huang, Z., Li, T., Morris, D., Finfrock, Z., Zhou, J., Jiao, M., Gao, J., et al. (2020b). Computationally aided, entropy-driven synthesis of highly efficient and durable multi-elemental alloy catalysts. Sci. Adv. *6*, 1–12, https://doi.org/10.1126/sciadv.aaz0510.

Ye, B., Fan, C., Han, Y., Ma, M., and Chu, Y. (2020). Synthesis of high-entropy diboride nanopowders via molten salt-mediated magnesiothermic reduction. J. Am. Ceram. Soc. *103*, 4738–4741, https://doi.org/10.1111/jace.17184.

Ye, Y.F., Wang, Q., Lu, J., Liu, C.T., and Yang, Y. (2016). High-entropy alloy: challenges and prospects. Mater. Today. https://doi.org/10.1016/j.mattod.2015.11.026.

Yeh, J.-W., Chen, S.-K., Lin, S.-J., Gan, J.-Y., Chin, T.-S., Shun, T.-T., Tsau, C.-H., and Chang, S.-Y. (2004). Nanostructured high-entropy alloys with multiple principal elements: novel alloy design concepts and outcomes. Adv. Eng. Mater. *6*, 299–303, https://doi.org/10.1002/adem.200300567.

Yuan, D., Liang, X., Wu, L., Cao, Y., Ai, X., Feng, J., and Yang, H. (2014). A honeycomb-layered Na 3 Ni 2 SbO 6 : a high-rate and cycle-stable cathode for sodium-ion batteries. Adv. Mater. *26*, 6301–6306, https://doi.org/10.1002/adma.201401946.

Yusenko, K.V., Riva, S., Carvalho, P.A., Yusenko, M.V., Arnaboldi, S., Sukhikh, A.S., Hanfland, M., and Gromilov, S.A. (2017). First hexagonal close packed high-entropy alloy with outstanding stability under extreme conditions and electrocatalytic activity for methanol oxidation. Scr. Mater. *138*, 22–27, https://doi.org/10.1016/j.scriptamat.2017.05.022.

Zhai, S., Rojas, J., Ahlborg, N., Lim, K., Toney, M.F., Jin, H., Chueh, W.C., and Majumdar, A. (2018). The use of poly-cation oxides to lower the temperature of two-step thermochemical water splitting. Energy Environ. Sci. *11*, 2172–2178, https://doi.org/10.1039/C8EE00050F.

Zhang, D., Zhao, H., Wu, X., Deng, Y., Wang, Z., Han, Y., Li, H., Shi, Y., Chen, X., Li, S., et al. (2020). Multi-site electrocatalysts boost pH-universal nitrogen reduction by high-entropy alloys. Adv. Funct. Mater. https://doi.org/10.1002/adfm.202006939.

Zhang, G., Ming, K., Kang, J., Huang, Q., Zhang, Z., Zheng, X., and Bi, X. (2018a). High entropy alloy as a highly active and stable electrocatalyst for hydrogen evolution reaction. Electrochim. Acta *279*, 19–23, https://doi.org/10.1016/j.electacta.2018.05.035.

Zhang, J., Yan, J., Calder, S., Zheng, Q., McGuire, M.A., Abernathy, D.L., Ren, Y., Lapidus, S.H., Page, K., Zheng, H., et al. (2019a). Long-range antiferromagnetic order in a rocksalt high entropy oxide. Chem. Mater. *31*, 3705–3711, https://doi.org/10.1021/acs.chemmater.9b00624.

Zhang, R.-Z., Gucci, F., Zhu, H., Chen, K., and Reece, M.J. (2018b). Data-driven design of ecofriendly thermoelectric high-entropy sulfides. Inorg. Chem. *57*, 13027–13033, https://doi.org/10.1021/acs.inorgchem.8b02379.

Zhang, Z., Yang, S., Hu, X., Xu, H., Peng, H., Liu, M., Thapaliya, B.P., Jie, K., Zhao, J., Liu, J., et al. (2019b). Mechanochemical nonhydrolytic sol-gel-strategy for the production of mesoporous multimetallic oxides. Chem. Mater. *31*, 5529–5536, https://doi.org/10.1021/acs.chemmater.9b01244.

Zhao, C., Ding, F., Lu, Y., Chen, L., and Hu, Y. (2020a). High-entropy layered oxide cathodes for sodium-ion batteries. Angew. Chem. Int. Ed. *59*, 264–269, https://doi.org/10.1002/anie.201912171.

Zhao, X., Xue, Z., Chen, W., Wang, Y., and Mu, T. (2020b). Eutectic synthesis of high-entropy metal phosphides for electrocatalytic water splitting. ChemSusChem *13*, 2038–2042, https://doi.org/10.1002/cssc.202000173.

Zheng, Y., Yi, Y., Fan, M., Liu, H., Li, X., Zhang, R., Li, M., and Qiao, Z.A. (2019). A high-entropy metal oxide as chemical anchor of polysulfide for lithium-sulfur batteries. Energy Storage Mater *23*, 678–683, https://doi.org/10.1016/j.ensm.2019.02.030.